

Radiating Electron Interaction with Multiple Colliding Electromagnetic Waves: Random Walk Trajectories, Lévy Flights, Limit Circles, and Attractors (Survey of the Structurally Determinate Patterns)

S. V. Bulanov^{1,2}, T. Zh. Esirkepov¹, S. S. Bulanov³, J. K. Koga¹, Z. Gong⁴, X. Q. Yan^{4,5}, and M. Kando¹

¹Kansai Photon Science Institute, National Institutes for Quantum and Radiological Science and Technology (QST), 8-1-7 Umemidai, Kizugawa, Kyoto 619-0215, Japan

²A. M. Prokhorov Institute of General Physics, the Russian Academy of Sciences, Vavilov street 38, 119991 Moscow, Russia

³Lawrence Berkeley National Laboratory, Berkeley, California 94720, USA

⁴State Key Laboratory of Nuclear Physics and Technology, and Key Laboratory of HEDP of the Ministry of Education, CAPT, Peking University, Beijing 100871, China

⁵Collaborative Innovation Center of Extreme Optics, Shanxi University, Taiyuan, Shanxi 030006, China
(Dated: January 13, 2017)

The multiple colliding laser pulse concept formulated in Ref. [1] is beneficial for achieving an extremely high amplitude of coherent electromagnetic field. Since the topology of electric and magnetic fields oscillating in time of multiple colliding laser pulses is far from trivial and the radiation friction effects are significant in the high field limit, the dynamics of charged particles interacting with the multiple colliding laser pulses demonstrates remarkable features corresponding to random walk trajectories, limit circles, attractors, regular patterns and Lévy flights. Under extremely high intensity conditions the nonlinear dissipation mechanism stabilizes the particle motion resulting in the charged particle trajectory being located within narrow regions and in the occurrence of a new class of regular patterns made by the particle ensembles.

PACS numbers: 52.38.-r, 41.60.-m, 52.27.Ep

CONTENTS

I. Introduction	2	2. Random-walk and regular patterns of the particle trajectories in the field of three s-polarized EM waves	13
II. Field configurations, dimensionless parameters and equations of motion	2	3. Ergodization or not?	15
A. N colliding EM waves	2	C. Electron interaction with three p-polarized EM waves	15
B. Dimensionless parameters characterizing interaction of laser radiation with charged particles	3	VI. Electron dynamics in four s- and p-polarized colliding EM pulses	16
C. Radiation friction force with the QED form-factor	5	A. S-polarized 4 colliding EM waves	16
III. Electron motion in the standing EM wave formed by two counter-propagating EM pulses	6	B. EM field configuration	16
A. EM field configuration	6	1. Particular solutions	16
B. Relatively weak intensity limit	6	2. General case	20
C. Random walk	7	C. Electron interaction with four p-polarized EM waves	22
D. Moderate intensity regime	8	VII. Conclusions	23
E. High intensity regime	8	Acknowledgments	27
IV. Simple model of the stabilization of the particle motion in an oscillating field due to the nonlinear friction	9	References	27
V. Regular and chaotic electron motion in three s- and p-polarized colliding laser pulses	12		
A. EM field configuration	12		
B. Electron interaction with three s-polarized EM waves	13		
1. Particular solutions	13		

I. INTRODUCTION

Recent progress in laser technology has lead to a dramatic increase of laser power and intensity. The lasers are capable of producing electromagnetic field intensities well above 10^{18}W/cm^2 , which corresponds to the relativistic quiver electron energy, and in the near future their radiation may reach intensities of 10^{24}W/cm^2 and higher [2]. As a result the laser-matter interaction will happen in the radiation friction dominated regimes [3–5]. In a strong electromagnetic field, electrons can be accelerated to such high velocities that the radiation reaction starts to play an important role [6–12]. Moreover, previously unexplored regimes of the interaction will be entered, in which quantum electrodynamics (QED) effects such as vacuum polarization, pair production and cascade development can occur [5, 13].

The electromagnetic field intensity of the order of 10^{24}W/cm^2 can be achieved in the focus of a $1\mu\text{m}$ wavelength laser of ten petawatt power. For 30 fs, i.e. for a ten wave period duration, the laser pulse energy is about 300 J. Within the framework of the multiple colliding laser pulses (MCLP) concept formulated in Ref. [1] (see Refs. [14–17] for development of this idea), the laser radiation with given energy \mathcal{E}_{las} is subdivided into several beams each of them having $1/N$ of the laser energy, where N is the number of the beams. If the beams interfere in the focus in a constructive way, i.e. their electric fields are summed, the resulting electric field and the laser intensity are equal to $E_N = \sqrt{N}E_{las}$ and to $I_N = NI_{las}$, respectively. Here E_{las} and I_{las} are the electric field and the intensity of the laser light. For a large number of beams there is a diffraction constraint on the electric field amplitude in the focus region. In the limit $N \rightarrow \infty$ the electromagnetic field can be approximated by the 3D dipole configurations (see [14]) for which the electric field maximum is given by [18]

$$E_m = 8\pi\sqrt{\frac{\mathcal{P}_{las}}{3c\lambda^2}}, \quad (1)$$

where \mathcal{P}_{las} , λ , and c are the laser power, wavelength, and speed of light in vacuum, respectively.

Since the radiation friction and QED processes both depend on the particle's momentum, the strength of the present electromagnetic field, and on their mutual orientation, it is crucial in understanding the dynamics of charged particles in the electromagnetic field in the regime of radiation dominance. Even in the simplest MCLP case, two counter-propagating plane waves, the particle behavior in the standing wave is quite complicated. It demonstrates regular and chaotic motion, random walk, limit circles and strange attractors as is shown by [19–29]. As is well known, the standing wave configuration is widely used in classical electrodynamics and in QED theory. This is due to the fact that in the planes where the magnetic field vanishes, the charged particle may be considered interacting with an oscillating pure electric field. This provides great simplification of the

theoretical description. In addition, as has been noted above, in a standing wave formed by two colliding laser pulses, the resulting EM field configuration facilitates QED effects (see [1, 30, 31]). Computer simulations presented in Refs. [32–34] show that the MCLP concept can be beneficial for realizing such important laser-matter interaction regimes as, for example, the electron-positron pair production via the Breit-Wheeler process [32] and the high efficiency gamma-ray flash generation due to nonlinear Thomson or multi-photon Compton scattering [33, 34]. Another configuration for the generation of a gamma-flash is a single laser pulse irradiating an overdense plasma target [35–38]. The applications of the laser based gamma-ray sources are reviewed in Ref. [39]. The radiation friction effects on ion acceleration, on magnetic field self-generation, and on high-order-harmonics in laser plasmas have been studied in Refs. [40], [41], and [42], respectively.

It is not surprising that the dynamics of the electron interacting with three-, four-, etc. colliding pulses is even more complicated and rich with novel patterns.

The present paper contains the theoretical analysis of the electron motion in the standing electromagnetic (EM) wave generated by two-, three-, and four colliding focused EM pulses. The paper is organized as follows. In next section we introduce the notations used, describe the field configurations and equations of motion and present the dimensionless parameters characterizing the charged particle interaction with a high intensity EM field. Then, in section 3 we briefly recover the main features of the electron motion in two counter-propagating plane waves. In section 4 we formulate a simple theoretical model of the stabilization of the particle motion in the oscillating field due to nonlinear dissipation effects, which explains the radiative electron trapping revealed earlier in Refs. [15, 16, 26–29, 43]. Section 5 relates to the regular and chaotic electron motion in three s-polarized laser pulses. The radiating electron dynamics in the four s- and p-polarized colliding EM pulses is discussed in section 6. Section 7 summarizes the conclusions.

II. FIELD CONFIGURATIONS, DIMENSIONLESS PARAMETERS AND EQUATIONS OF MOTION

A. N colliding EM waves

Consider N monochromatic plane waves in vacuum with the same frequencies ω_0 and equal amplitudes a_n . We assume that the wave vectors \mathbf{k}_n are in the (x, y) plane. The wave vector of the n th wave is equal to

$$\mathbf{k}_n = k_0[\sin(\theta_n)\mathbf{e}_x + \cos(\theta_n)\mathbf{e}_y], \quad (2)$$

where $k_0 = \omega_0/c$, $\theta_n = 2\pi(n-1)/N$, $n = 1, 2, 3, \dots, N$, and \mathbf{e}_x and \mathbf{e}_y are unit vectors in the x and y directions.

It is convenient to describe the s-polarized EM waves with the electric field normal to the (x, y) plane, i.e. $\mathbf{E} =$

$E_z \mathbf{e}_z$ with the unit vector \mathbf{e}_z along the z direction, in terms of $E_z(x, y, t)$ equal to

$$E_z = E_n \sum_{n=1}^N \sin \left\{ \omega_0 \left[t - \frac{\sin(\theta_n)x - \cos(\theta_n)y}{c} \right] \right\}. \quad (3)$$

Here the amplitude of the n_{th} wave is $E_n = E_0/\sqrt{N}$ where $E_0 = E_{las}$. The magnetic field can be expressed by using Maxwell's equations: $(1/c)\partial_t B_x = -\partial_y E_z$ and $(1/c)\partial_t B_y = \partial_x E_z$.

In the case of p-polarized EM waves with the magnetic field normal to the (x, y) plane, $\mathbf{B} = B_z \mathbf{e}_z$, the B_z field of colliding N pulses is given by

$$B_z = B_n \sum_{n=1}^N \cos \left\{ \omega_0 \left[t - \frac{\sin(\theta_n)x - \cos(\theta_n)y}{c} \right] \right\} \quad (4)$$

with $B_n = E_{las}/\sqrt{N}$ and the electric field components expressed via Maxwell's equations as $(1/c)\partial_t E_x = \partial_y B_z$ and $(1/c)\partial_t E_y = -\partial_x B_z$, respectively.

B. Dimensionless parameters characterizing interaction of laser radiation with charged particles

Introducing the normalized variables, we change the space and time coordinates to $x/\lambda \rightarrow x$ and $t\omega/2\pi \rightarrow t$.

The interaction of charged particles with intense EM fields is characterized by several dimensionless and relativistic invariant parameters ([5, 26, 44]).

The first parameter is

$$a = \frac{e\sqrt{A_\mu A^\mu}}{m_e c^2}, \quad (5)$$

where A^μ is the 4-potential of the electromagnetic field with $\mu = 0, 1, 2, 3, 4$. Here and below summation over repeating indexes is assumed. This parameter is relativistically invariant for a plane EM wave. It is related to the wave normalized amplitude introduced above. When it is equal to unity, i.e. the intensity of a linearly polarized EM wave is $I_R = 1.37 \times 10^{18} (1\mu m/\lambda)^2 \text{ W/cm}^2$, the quiver electron motion becomes relativistic.

The ratio, $eE/m_e \omega c$, the dimensionless EM field amplitude, measures the work in units of $m_e c^2$ produced by the field on an electron over the distance equal to the field wavelength. Here, e and m_e are the charge and mass of an electron, E and ω are the EM field strength and frequency, and c is the speed of light.

The second dimensionless parameter is ε_{rad} :

$$\varepsilon_{rad} = \frac{4\pi r_e}{3\lambda} = 1.18 \times 10^{-8} \left(\frac{1\mu m}{\lambda} \right), \quad (6)$$

which is proportional to the ratio of the classical electron radius $r_e = e^2/m_e c^2 = 2.8 \times 10^{-13} \text{ cm}$ to the laser radiation wavelength, λ . It essentially determines the strength

of the radiation reaction effects for an electron radiating an EM wave.

When one micron wavelength laser intensities exceed 10^{23} W/cm^2 , the nonlinear quantum electrodynamics effects begin to play a significant role in laser plasma interactions (e.g. see Ref. [26] and literature cited therein). These effects manifest themselves through multi-photon Compton and Breit-Wheeler effects [44–46] (see Refs.: [47–55] for recent studies), i.e., through either photon emission by an electron or positron, or electron-positron pair production by a high energy photon, respectively. The multi-photon Compton and Breit-Wheeler processes are characterized in terms of two dimensionless relativistic and gauge invariant parameters [44]:

$$\chi_e = \frac{\sqrt{|F^{\mu\nu} p_\nu|^2}}{E_S m_e c} \quad \text{and} \quad \chi_\gamma = \frac{\lambda_C \sqrt{|F^{\mu\nu} k_\nu|^2}}{E_S}. \quad (7)$$

where p_ν and $\hbar k_\nu$ denote the 4-momenta of an electron or positron undergoing the Compton process and a photon undergoing the Breit-Wheeler process, the 4-tensor of the electromagnetic field is defined as $F_{\mu\nu} = \partial_\mu A_\nu - \partial_\nu A_\mu$, with the critical QED electric field

$$E_S = \frac{m_e^2 c^3}{e \hbar}. \quad (8)$$

This field is also known as the ‘‘Schwinger field’’ [56]. Its amplitude is about 10^{18} V/cm , which corresponds to the radiation intensity $\approx 10^{29} \text{ W/cm}^2$. The work produced by the field E_S on an electron over the distance equal to the reduced Compton wavelength, $\lambda_C = \hbar/m_e c = 3.86 \times 10^{-11} \text{ cm}$ equals $m_e c^2$. Here \hbar is the reduced Planck constant.

In 3D notation the parameter χ_e given by Eq. (7) reads

$$\chi_e = \frac{\gamma_e}{E_S} \sqrt{\left(\mathbf{E} + \frac{\mathbf{p}_e \times \mathbf{B}}{m_e c \gamma_e} \right)^2 - \left(\frac{\mathbf{p}_e \cdot \mathbf{E}}{m_e c \gamma_e} \right)^2}. \quad (9)$$

For the parameter χ_γ defined by Eq. (7) we have

$$\chi_\gamma = \frac{\hbar}{E_S m_e c} \sqrt{\left(\frac{\omega_\gamma}{c} \mathbf{E} + \mathbf{k}_\gamma \times \mathbf{B} \right)^2 - (\mathbf{k}_\gamma \cdot \mathbf{E})^2}. \quad (10)$$

Here γ_e , \mathbf{p}_e , ω_γ and \mathbf{k}_γ correspond to the representation of the electron 4-momentum p_ν and of the photon 4-wavenumber k_ν as $p_\nu = (\gamma_e m_e c, \mathbf{p})$ and $k_\nu = (\omega_\gamma/c, \mathbf{k}_\gamma)$, respectively. The parameter χ_e can also be defined as the ratio of the electric field to the critical electric field of quantum electrodynamics, E_S , in the electron rest frame. In particular, it characterizes the probability of the gamma-photon emission by an electron with 4-momentum p_ν in the field of the electromagnetic wave, in the Compton scattering process.

The parameter χ_γ characterizes the probability of the electron-positron pair creation by the photon with the momentum $\hbar k_\nu$ interacting with a strong EM wave in the Breit-Wheeler process.

The probabilities of the Compton scattering and of the Breit-Wheeler processes depend strongly on χ_e and χ_γ , reaching optimal values when $\chi_e \sim 1$ and $\chi_\gamma \sim 1$ ([44]).

In the case of an electron interaction with a plane EM wave propagating along the x -axis with phase and group velocity equal to speed of light in vacuum the parameters of the interaction can be written in terms of EM field strength, normalized by the QED critical field given by Eq. (8), and either the electron γ_e -factor or the photon energy $\hbar\omega_\gamma$:

$$\chi_e = \frac{E}{E_S} \left(\gamma_e - \frac{p_x}{m_e c} \right) \quad (11)$$

and

$$\chi_\gamma = \frac{E}{E_S} \frac{\hbar(\omega_\gamma - k_{\gamma,x}c)}{m_e c^2}. \quad (12)$$

For an electron interacting with the EM wave the linear combination of the electron energy and momentum,

$$h_e = \gamma_e - p_x/m_e c, \quad (13)$$

on r.h.s. of Eq. (11) is an integral of motion ([57]). Its value is determined by initial conditions.

If an electron/positron or a photon co-propagates with the EM wave, then in the former case the parameter χ_e is suppressed by a factor $(2\gamma_{e,0})^{-1}$, i.e. $\chi_e \simeq (2\gamma_{e,0})^{-1}(E/E_S)$, where $\gamma_{e,0}$ is the electron gamma-factor before interaction with the laser pulse. In the later case, when the gamma-photon co-propagates with the EM wave, the parameter χ_γ is equal to zero, $\chi_\gamma = 0$, because $\omega_\gamma = k_{\gamma,x}c$. On the contrary, the parameter χ_e can be enhanced to approximately $2\gamma_{e,0}E/E_S$, when the electron interacts with a counter-propagating laser pulse. Therefore the head-on collision configuration has an apparent advantage for strengthening the electron-EM-wave interaction and, in particular, for enhancing the γ ray production due to nonlinear Thomson or/and Compton scattering.

Depending on the energy of charged particles and field strength the interaction happens in one of the following regimes parametrized by the values of a , χ_e , and χ_γ :

- (i) $a > 1$, the relativistic interaction regime ([3]),
- (ii) $a > \varepsilon_{rad}^{-1/3}$, the interaction becomes radiation dominated ([7, 8, 58]),
- (iii) $\chi_e \geq 1$ the quantum effects begin to manifest themselves ([26, 59, 60]), and
- (iv) $\chi_e > 1$, $\chi_\gamma > 1$ marks the condition for the EM avalanche ([14, 61–64]), which is the phenomenon of exponential growth of the number of electron-positrons and photons in the strong EM field, being able to develop. These conditions can be supplemented by $\alpha a > 1$, which indicates that the number of photons emitted incoherently per laser period can be larger than unity as has been noted by [59]. Here the parameter ε_{rad} is given by Eq. (6) and $\alpha = e^2/\hbar c \approx 1/137$ is the fine structure constant.

As one can see two dimensionless parameters, a and χ_e , can be used to subdivide the (a, χ_e) plane into four domains shown in Fig. 1 a) (see also Refs. [26, 65]). The $\chi_e = 1$ line divides the plane into the radiation reaction description of the interaction domain ($\chi_e < 1$) and QED description of interaction domain ($\chi_e > 1$). The $a = \varepsilon_{rad}^{-1/3}$ line divides the plane into radiation dominated ($a > \varepsilon_{rad}^{-1/3}$) and particle dominated ($a < \varepsilon_{rad}^{-1/3}$) regimes of interaction domains. We note that the $a = \varepsilon_{rad}^{-1/3}$ threshold comes from the requirement for an electron to emit the amount of energy per EM wave period equal to the energy gain from the EM wave during the wave period. If one takes into account the discrete nature of the photon emission, then the same condition will take the form $a m_e c^2 = \hbar\omega_\gamma(\lambda/L_R)$ [46], where L_R is the radiation length. It is of the order of [66]

$$L_R = \lambda_\gamma \gamma_e^2. \quad (14)$$

In the limit $\chi_e \ll 1$, when $\lambda_\gamma \approx \lambda/\gamma_e^3$ and $\gamma_e \approx a$ we have $L_R \approx 2\lambda/a$. For $\chi_e \gg 1$ the radiation length is $L_R \approx \lambda \gamma_e^{1/3}/a^{2/3}$ as shown in Refs. [44–46]. This condition in the limit $\chi_e \rightarrow 0$ tends to the classical limit $a = \varepsilon_{rad}^{-1/3}$.

The intersection point, where $a_{rad} = \varepsilon_{rad}^{-1/3}$ and the parameter χ_e is equal to unity, determines critical values of the EM wave amplitude $\varkappa_a a^*$ with

$$a^* = \left(\frac{3c}{2r_e \omega^*} \right)^{1/3} = \frac{\hbar c}{e^2} = \frac{1}{\alpha}, \quad (15)$$

i. e. the wave electric field is $\varkappa_a \varkappa_\omega E^*$, where

$$E^* = E_S \alpha, \quad (16)$$

and the wave frequency $\varkappa_\omega \omega^*$ with ω^* given by

$$\omega^* = \frac{e^4 m_e}{\hbar^3} = \frac{m_e c^2}{\hbar \alpha^2}. \quad (17)$$

Here $\alpha = 1/137$ is the fine structure constant, and \varkappa_a and \varkappa_ω are constants of the order of unity. The normalized EM wave amplitude equals $a^* = 137$ with corresponding the wave intensity $I^* = 2.6 \times 10^{22} \text{ W/cm}^2$. The corresponding photon energy is $\hbar\omega^* = m_e c^2/\alpha^2 \approx 27 \text{ eV}$. We note that the value of $a^* = 1/\alpha$ corresponds to the one of conditions for the charged particle interaction with EM field to be in the QED regime, $\alpha a > 1$ (see also [59]).

Concrete values of the coefficients \varkappa_a and \varkappa_ω depend on the specific electromagnetic configuration. For example, in the case of a rotating homogeneous electric field (it can be formed in the antinodes of an electric field in the standing EM wave) analyzed in Ref. [26], they are $\varkappa_a = 3$ and $\varkappa_\omega = 1/18$, respectively, which gives $\varkappa_a a^* = 411$, with the intensity equal to $2.3 \times 10^{23} \text{ W/cm}^2$, and $\varkappa_\omega \hbar\omega^* = m_e c^2 \alpha^2/18 \approx 1.5 \text{ eV}$.

Here we would like to attract attention to the relationship between the well known critical electric field of

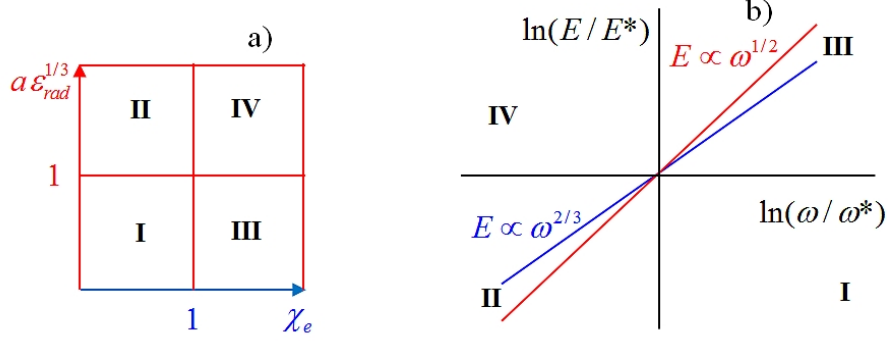


FIG. 1. Regimes of electromagnetic field interaction with matter on the plane of parameters: a) the normalized EM wave amplitude $a\varepsilon_{rad}^{1/3}$ and the parameter χ_e ; b) accordingly the $(\ln(E/E^*), \ln(\omega/\omega^*))$ plane, where E^* and ω^* are given by Eqs. (16) and (17), respectively. The parameter planes are subdivided into 4 domains: (I) Electron - EM field interaction in the particle dominated radiation reaction domain; (II) Electron - EM field interaction is dominated by the radiation reaction; (III) Electron - EM field interaction is in the particle dominated QED regime; (IV) Electron - EM field interaction is in the radiation dominated QED regime.

classical electrodynamics E_{cr} , the critical electric field of quantum electrodynamics E_S and the electric field E^* . They can be written as $E_{cr} = e/r_e^2$, $E_S = e/r_e \lambda_C$, and $E^* \approx e/\lambda_C^2$, respectively. In other words we have $E_S = E_{cr}\alpha$, and $E^* = E_{cr}\alpha^2$.

Using the relationships obtained above we find that on the line $a\varepsilon_{rad}^{1/3} = 1$ the wave electric field is proportional to the frequency in the 2/3 power, i. e. $E/E^* = (\omega/\omega^*)^{2/3}$, and on the line $\chi_e = 1$ we have $E/E^* = (\omega/\omega^*)^{1/2}$.

Fig. 1 b) shows the $(\ln(E/E^*), \ln(\omega/\omega^*))$ plane with 4 domains. The lines intersect each other at the point $(0, 0)$, i.e. at the point where $E = E^*$ and $\omega = \omega^*$.

C. Radiation friction force with the QED form-factor

In order to describe the relativistic electron dynamics in the electromagnetic field we shall use the equations of electron motion:

$$\frac{d\mathbf{p}}{dt} = e \left(\mathbf{E} + \frac{\mathbf{v}}{c} \times \mathbf{B} \right) + F_{rad}, \quad (18)$$

$$\frac{d\mathbf{x}}{dt} = \frac{\mathbf{p}}{m_e \gamma}, \quad (19)$$

where the radiation friction force, $F_{rad} = G_e \mathbf{f}_{rad}$, is the product of the classical radiation friction force, \mathbf{f}_{rad} , in the Landau-Lifshitz form ([57]):

$$\mathbf{f}_{rad} = \frac{2e^3}{3m_e c^3 \gamma} \left\{ (\partial_t + (\mathbf{v} \nabla) \mathbf{E} + \frac{1}{c} [\mathbf{v} \times (\partial_t + (\mathbf{v} \nabla) \mathbf{B})] \right\} + \frac{2e^4}{3m_e^2 c^4} \left\{ \mathbf{E} \times \mathbf{B} + \frac{1}{c} [\mathbf{B} \times (\mathbf{B} \times \mathbf{v}) + \mathbf{E} (\mathbf{v} \cdot \mathbf{E})] \right\} \quad (20)$$

$$- \frac{2e^4}{3m_e^2 c^5} \gamma^2 \mathbf{v} \left\{ \left(\mathbf{E} + \frac{1}{c} \mathbf{v} \times \mathbf{B} \right)^2 - \frac{1}{c^2} (\mathbf{v} \cdot \mathbf{E})^2 \right\}$$

and a form-factor G_e , which takes into account the quantum electrodynamics weakening of the radiation friction [56, 67–70]. Discussions of the relationship between the Landau-Lifshitz and Lorentz-Abraham-Dirac forms of the radiation friction force and what form of the force follows from the QED calculation, can be found in Refs. [71–73] and in the literature cited therein.

As we have noted above, the threshold of the QED effects is determined by the dimensionless parameter χ_e given by Eq. (9). For example, if an electron moves in the magnetic field B , the parameter is equal to $\chi_e \approx \gamma_e (B/B_S)$, where $B_S = m_e^2 c^3 / e \hbar$ is the QED critical magnetic field (see also Eq. (8)). The energy of the emitted synchrotron photons is

$$\hbar \omega_\gamma = m_e c^2 \gamma_e \frac{\chi_e}{2/3 + \chi_e}. \quad (21)$$

In the limit $\chi_e \ll 1$ the frequency ω_γ is equal to $(3/2) \omega_{Be} \gamma_e^2$ in accordance with classical electrodynamics (see [57]). Here $\omega_{Be} = eB/m_e c$ is the Larmor frequency. If $\chi_e \gg 1$ the photon energy is equal to the energy of the radiating electron: $\hbar \omega_\gamma = m_e c^2 \gamma_e$.

The radiation friction force in the limit $\gamma_e \rightarrow \infty$, i.e. the last term on the r.h.s. of Eq. (20) retained, can be written in the following form (see also Refs. [26, 67–70] and literature cited therein)

$$\mathbf{f}_{rad} = - \frac{2 \alpha c G_e(\chi_e) \chi_e^2}{3 \lambda_C} \mathbf{p}. \quad (22)$$

Here the QED effects are incorporated into the equations of the electron motion by using the form-factor $G_e(\chi_e)$

(see Ref. [67]), which is equal to the ratio of full radiation intensity to the intensity of the radiation emitted by a classical electron. It reads

$$G_e(\chi_e) = \frac{3}{4} \int_0^\infty \left[\frac{4 + 5\chi_e x^{3/2} + 4\chi_e^2 x^3}{(1 + \chi_e x^{3/2})^4} \right] \Phi'(x) x dx, \quad (23)$$

where $\Phi(x)$ is the Airy function ([74]). In Eq. (22) we neglect the effects of the discrete nature of the photon emission in quantum electrodynamics (see [12, 25, 27, 28, 64, 75, 76]).

In the limit $\chi_e \ll 1$ the form-factor $G(\chi_e)$ tends to unity as

$$\begin{aligned} G_e(\chi_e) &= 1 - \frac{55\sqrt{3}}{16} \chi_e + 48\chi_e^2 + \dots \\ &\approx 1 - 5.95\chi_e + 48\chi_e^2 + \dots \end{aligned} \quad (24)$$

For $\chi_e \gg 1$ it tends to zero as

$$\begin{aligned} G_e(\chi_e) &= \frac{32\pi}{27 \cdot 3^{5/6} \Gamma(1/3) \chi_e^{4/3}} - \frac{1}{\chi_e^2} + \dots \\ &\approx \frac{0.5564}{\chi_e^{4/3}} - \frac{1}{\chi_e^2} + \dots \end{aligned} \quad (25)$$

However expression (23) and the asymptotical dependences (25) and (26) are not convenient for implementing them in the computer codes. For the sake of calculation simplicity we shall use the following approximation

$$G_R(\chi_e) \approx \frac{1}{(1 + 8.93\chi_e + 2.41\chi_e^2)^{2/3}}. \quad (26)$$

Within the interval $0 < \chi_e < 10$ the accuracy of this approximation is better than 1%.

III. ELECTRON MOTION IN THE STANDING EM WAVE FORMED BY TWO COUNTER-PROPAGATING EM PULSES

A. EM field configuration

An electron interaction with an EM field formed by two counter-propagating waves was addressed a number of times in high field theory using classical quantum electrodynamics approaches because it provides one of the basic EM configurations where important properties of a radiating electron can be revealed (e.g. see above cited publications [5, 16, 19, 22–29, 77–80]). Here we present the results of the analysis of an electron motion in a standing EM wave in order to compare them below with the radiating electron behavior in a more complicated EM configuration formed by three and four waves with various polarizations.

Here we consider an electron interaction with the electromagnetic field corresponding to two counter-propagating linearly polarized waves of equal amplitudes,

$(a_0/2) \cos(t+x)$ and $(a_0/2) \cos(t-x)$, forming a standing wave. The field is given by the electromagnetic 4-potential

$$\mathbf{A} = a_0 \cos t \cos x \mathbf{e}_z. \quad (27)$$

This is a standing electromagnetic wave with zero magnetic and electric field nodes located at the coordinates $x = \pm\pi n$ and $x = \pm\pi(n + 1/2)$ with $n = 0, 1, 2, \dots$, respectively.

Numerical integration of the electron motion equations with the radiation friction force in the form (22) shows different features of the electron dynamics depending on the electromagnetic wave amplitude and the dissipation parameter ε_{rad} .

B. Relatively weak intensity limit

In the limit of relatively weak dissipation, which corresponds to the domain I in Fig. 1, the electron trajectory wanders in the phase space and in the coordinate space as shown in Fig. 2. In this case the wave amplitude is $a_0 = 618$. The dissipation parameter equals $\varepsilon_{rad} = 2 \times 10^{-8}$. The normalized critical QED field is $a_S = eE_S/m_e\omega c = m_e c^2/\hbar\omega = 4 \times 10^5$. The parameter values correspond to the vicinity of the point $(a/a^* = 1, \omega/\omega^* = 1)$ in Fig. 1 b). The integration time equals 75.

Fig. 2 demonstrates a typical behavior of the electron in the limit of relatively low EM wave amplitude. Fig. 2 a) and b) show that the electron performs a random-walk-like motion for a long time being intermittently trapped and untrapped in the vicinities of the zero-electric field nodes, where the electric field vanishes. For this parameter choice the equilibrium trajectory at the electric field antinodes is unstable according to Ref. [14] (see also [81]). The maximum value of the electron gamma-factor, γ_e , whose dependence on the coordinate x is plotted in Fig. 2 c), reaches 700. In the oscillating electric field of amplitude $a = 618$ it would be equal to 618. The parameter χ_e (see Fig. 2 d)) changes between zero and approximately 0.7, which corresponds within an order of magnitude to $(a_0/a_S)\gamma_e$. The particle coordinates z versus time space in Fig. 3 for initial coordinates $x(0) = 0.01-1, 0.2-2, 0.49-3$ with other parameters the same as in Fig. 2 show their wandering along the coordinate z . The particle over-leaping from one field period to another with small scale oscillations in between seen in Fig. 3 may correspond to Lévy flights (see [82–85]).

Fig. 4, shows the Poincaré section for the motion of the particle with $x(0) = 0.01$ positions in the phase plane (p_x, p_z) at discrete times with the time step equal to the period of the driving force. The parameters are the same as in Fig. 2. The Poincaré section demonstrates that this process is stochastic.

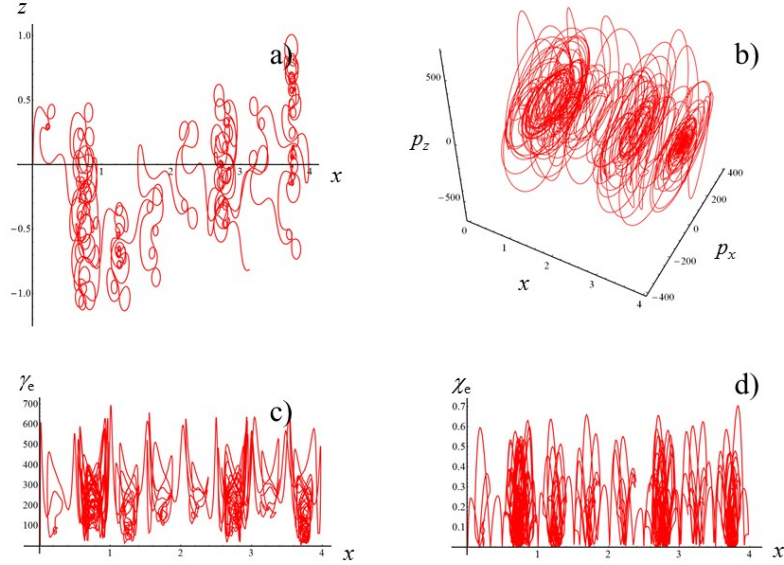


FIG. 2. a) Electron trajectories in the (x, z) plane for initial conditions: $x(0) = 0.01$, $z(0) = 0$, $p_x(0) = 0$, $p_z(0) = 0$. b) Trajectory in the phase space x, p_x, p_z ; c) Electron gamma-factor γ_e versus the coordinate x ; d) Parameter χ_e versus the coordinate x , for the same initial conditions. The electromagnetic field amplitude is $a_0 = 617$ and the dissipation parameter is $\varepsilon_{rad} = 1.2 \times 10^{-8}$. The coordinates, time and momentum are measured in the $2\pi c/\omega$, $2\pi/\omega$ and $m_e c$ units.

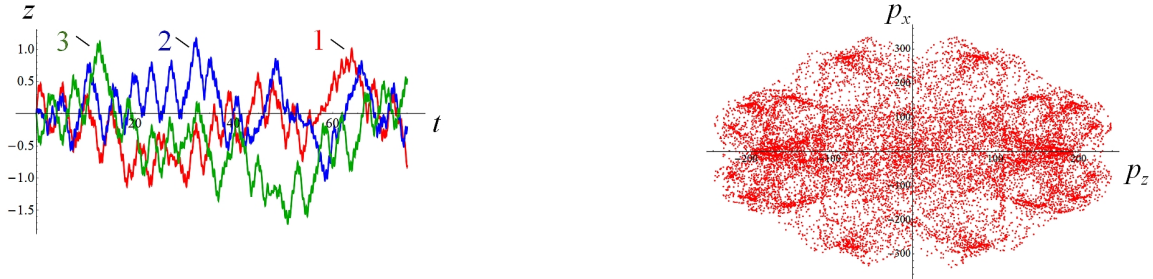


FIG. 3. Electron coordinate z versus time space for initial coordinates $x(0) = 0.01-1$, $0.2-2$, $0.49-3$, other parameters are the same as in Fig. 2.

C. Random walk

Now we analyze the time dependence of the random walk, assuming that the particle coordinates $x(t)$ and $z(t)$ are random variables, i.e. the particle displacement in the (x, z) plane equal to $r = \sqrt{x^2 + z^2}$ is also a random variable. As is known in statistics the behavior of the random variable f is characterized by the expectation $\mu = E[f]$ and variance $\sigma^2 = \text{Var}[f]$ defined as

$$E[f] = \lim_{t \rightarrow \infty} \frac{1}{t} \int_0^t f(t) dt \quad (28)$$

and

$$\text{Var}[f] = E[(f - E[f])^2]. \quad (29)$$

The definition of an expectation in the form (28) implies that the probability density function is taken to be a continuous uniform distribution equal to $1/t$ within the interval $[0, t]$. We assume here that the ergodicity of the processes is expected.

If the random walk process is a Wiener process, which also called “Brownian motion”, the variance of the walker’s coordinate $r(t)$ is proportional to time (e.g. see

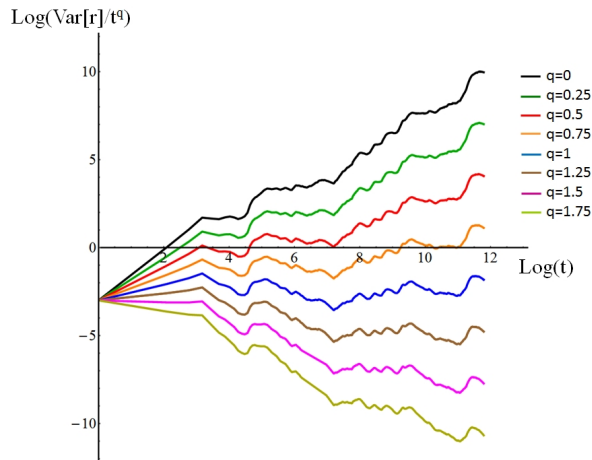


FIG. 5. Dependences of $\text{Log}(\text{Var}[r]/t^q)$ on $\text{Log}(t)$ for $0 < q < 1.25$ for the parameters corresponding to Fig. 2.

[86]). To examine whether or not the random walk seen in Figs. 2 and 3 is a Wiener process we plot in Fig. 5 the dependences of $\text{Log}(\text{Var}[r]/t^q)$ on $\text{Log}(t)$ for $0 < q < 1.75$. For the Wiener process the parameter q should be equal to 1. As we can see, in our case random walk process the variance is proportional to t^q with $q \approx 1$.

D. Moderate intensity regime

The situation qualitatively changes, when the dissipation becomes more significant. In Fig. 1 this corresponds to the domain II. This case is illustrated in Fig. 6, for which the radiation friction parameter is $\varepsilon_{rad} = 6 \times 10^{-9}$, the normalized critical QED field is $a_S = 8 \times 10^5$, and the normalized laser field equals $a_0 = 778$. In Fig. 6 we present three trajectories for particles with initial conditions: $x(0) = 0.01, z(0) = 0, p_x(0) = 0, p_z(0) = 0$ (red); $x(0) = 0.2, z(0) = 0, p_x(0) = 0, p_z(0) = 0$ (blue); $x(0) = 0.49, z(0) = 0, p_x(0) = 0, p_z(0) = 0$ (green). As seen in Fig. 6 a), where the trajectories in the x, z plane are shown, independent of the initial position all three trajectories end up in the vicinity of the plane $x = 0.25$. Here the EM wave electric field vanishes.

At the coordinate $x = 0.25$ the ponderomotive potential has a minimum. It is defined as

$$\Pi(x) = \frac{1}{2\pi} \int_{-\pi}^{\pi} (\sqrt{1 + A(x, t)^2} - 1) dt \quad (30)$$

with the vector potential $A(x, t)$ given by Eq. (27). The dashed curve in Fig. 6 a) presents the ponderomotive potential (30) dependence on the x coordinate. In Fig. 6 b) electron trajectories in the (x, p_x, p_z) space show the attractors, which have been analyzed in details in Ref. [27] (see Fig. 7, where the Poincaré section is presented for this case). Electron gamma-factors γ_e versus the coordinate x presented in Fig. 6 c) correspond to

the case when the dissipation limits the particle energy, which does not exceed the value determined by the amplitude of the EM wave being of the order of a . Since the parameter $\chi_e(x)$ plotted in Fig. 6 d) is less than unity for all three trajectories, the equation of an electron motion with the radiation friction force is still valid for this parameter range.

In Fig. 7, we plot the Poincaré section for the particle with the same parameters as in Fig. 6 for $x(0) = 0.01$. Here are the particle positions in the phase plane (x, p_x) at discrete times with the time step equal to the period of the driving force. The map pattern corresponds to the stochastic regime developed in the particle motion.

E. High intensity regime

If we choose the parameters in a such the way that the dissipation becomes even more significant, when we approach the domain IV in Fig. 1, the particle behavior becomes counterintuitive, as can be seen in Fig. 8, for which the radiation friction parameter is $\varepsilon_{rad} = 1.2 \times 10^{-9}$, the normalized critical QED field is $a_S = 4 \times 10^6$, and the normalized laser field equals $a_0 = 1996$. There we present three electron trajectories for the same initial conditions as in Fig. 4: $x(0) = 0.01, z(0) = 0, p_x(0) = 0, p_z(0) = 0$ (red); $x(0) = 0.2, z(0) = 0, p_x(0) = 0, p_z(0) = 0$ (blue); $x(0) = 0.49, z(0) = 0, p_x(0) = 0, p_z(0) = 0$ (green). Trajectories in the x, z plane (Fig. 6 a)) are principally different depending on where the particle has been initially localized. For $x(0) = 0.2$ the trajectory remains in the vicinity of the ponderomotive potential minimum similarly to the case discussed above (Fig. 6). The dashed line is the ponderomotive potential (30) vs the x coordinate. In contrast, particles with initial coordinates near the maximum of the ponderomotive potential are trapped there (similar behavior was noted in Ref. [24]).

In Fig. 8 b) the electron trajectories in the (x, p_x, p_z) space show behaviour typical for limit circles and attractors. The inset shows the zoomed trajectory for $x(0) = 0.2$ corresponding to a strange attractor [27]. The trajectories with $x(0) = 0.01$ and $x(0) = 0.49$ demonstrate regular limit circles. It follows from Fig. 8 c) that the electron gamma-factor γ_e has a moderate value for the electron trapped near the ponderomotive potential minimum (the inset shows zoomed $\gamma_e(x)$ for $x(0) = 0.2$), and the particles are efficiently accelerated when they are trapped in the region at the ponderomotive potential maximum. For the parameters chosen $\chi_e(x)$ plotted in Fig. 8 d) remains less than unity for all three trajectories, i. e. the QED effects are finite but relatively weak.

In Fig. 9, we plot the Poincaré section showing the particle with $x(0) = 0.49$ positions in the phase plane (x, p_x) at discrete times with the time step equal to the period of the driving force. The parameters are the same as in Fig. 8 for $x(0) = 0.49$. Although the map pattern is pretty complicated it does not contain curve broadening, i.e. does not indicate a stochastic regime of the particle

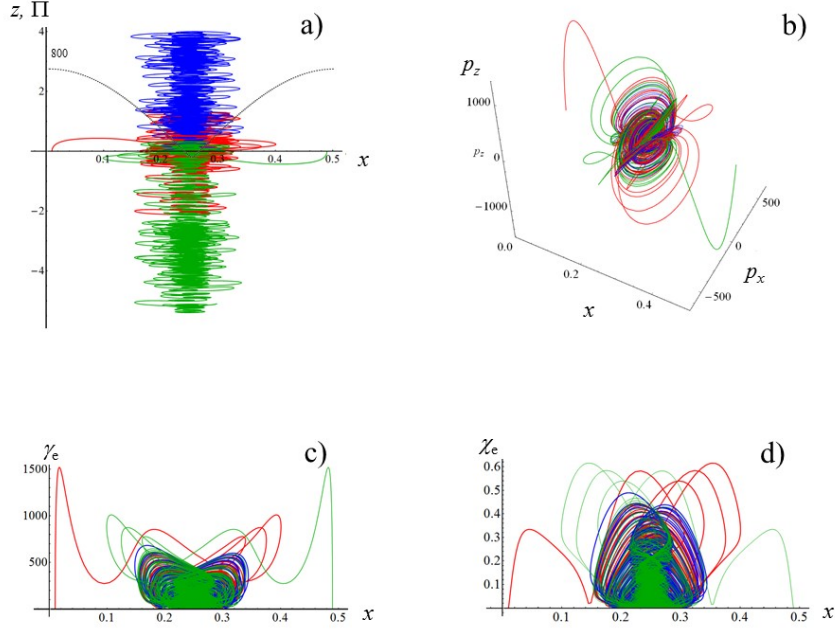


FIG. 6. Electron motion in the standing EM wave for $\varepsilon_{rad} = 6 \times 10^{-9}$, $a_S = 8 \times 10^5$, and $a_0 = 778$ for initial conditions: $x(0) = 0.01$, $z(0) = 0$, $p_x(0) = 0$, $p_z(0) = 0$ (red); $x(0) = 0.2$, $z(0) = 0$, $p_x(0) = 0$, $p_z(0) = 0$ (blue); $x(0) = 0.49$, $z(0) = 0$, $p_x(0) = 0$, $p_z(0) = 0$ (green). a) Trajectory in the x, z plane. Dashed line is the ponderomotive potential (30) vs the x coordinate; b) Electron trajectories in the (x, p_x, p_z) space. c) Electron gamma-factor γ_e versus the coordinate x . d) Parameter χ_e versus the coordinate x , for the same initial conditions.

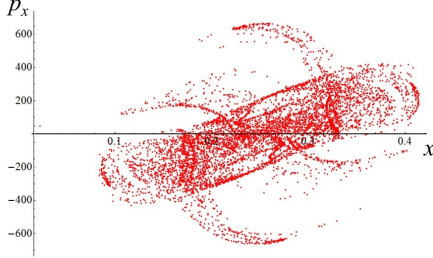


FIG. 7. The Poincaré sections showing the particle positions in the phase plane (x, p_x) at discrete times with the time step equal to the period of the driving force. The parameters are the same as in Fig. 6 for $x(0) = 0.01$.

motion.

In the next Section we discuss the mechanism of dissipative particle trapping in the vicinity of the ponderomotive potential maximum, which can explain the observed effects (see also [87]).

IV. SIMPLE MODEL OF THE STABILIZATION OF THE PARTICLE MOTION IN AN OSCILLATING FIELD DUE TO THE NONLINEAR FRICTION

Let us consider a particle motion in a fast oscillating field in a way similar to [88]. As in Ref. [88] for the sake of simplicity of calculations we assume non-relativistic electron motion in one dimension, when the force acting on the particle depends on the coordinate x and time t . In contrast to the consideration in Ref. [88], we take into account the effects of the friction. The equation of particle motion is

$$\ddot{x} + \kappa(F)\dot{x} = F. \quad (31)$$

Here a dot stands for the time derivative and $\kappa(F)$ is the friction coefficient. It is assumed to depend on the rapidly oscillating driving force,

$$F(x, t) = f_1(x) \cos \omega t + f_2(x) \sin \omega t. \quad (32)$$

We seek a solution of Eq. (31), assuming that it can be written down as a sum of two parts,

$$x(t) = X(t) + \xi(t), \quad (33)$$

where $X(t)$ slowly varies with time and $\xi(t)$ is a small fast oscillating periodic function, $|\xi| \ll |X|$.

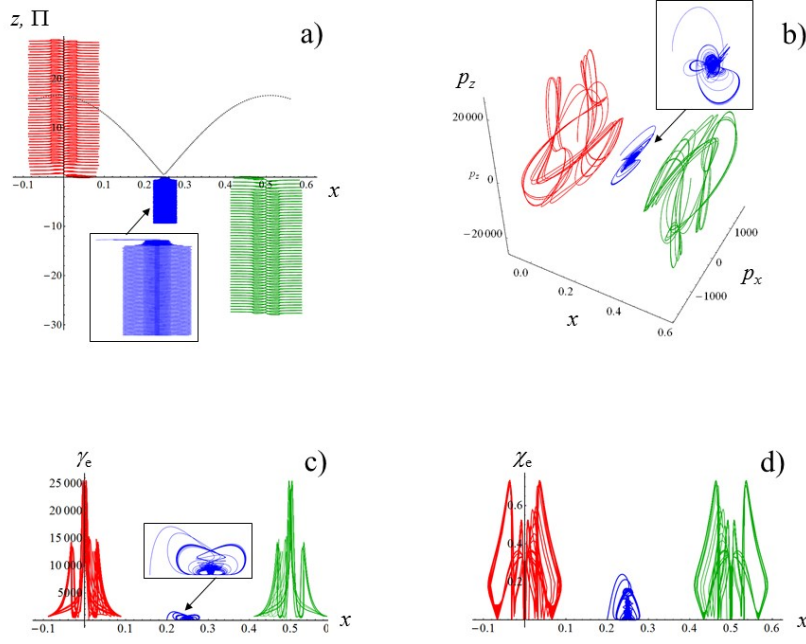


FIG. 8. Electron motion in the standing EM wave for $\varepsilon_{rad} = 1.2 \times 10^{-9}$, $a_S = 4 \times 10^6$, $a = 1996$ for initial conditions: $x(0) = 0.01$, $z(0) = 0$, $p_x(0) = 0$, $p_z(0) = 0$ (red); $x(0) = 0.2$, $z(0) = 0$, $p_x(0) = 0$, $p_z(0) = 0$ (blue); $x(0) = 0.49$, $z(0) = 0$, $p_x(0) = 0$, $p_z(0) = 0$ (green). a) Trajectory in the x, z plane. Inset shows zoomed trajectory for $x(0) = 0.2$. Dashed line is the ponderomotive potential (30) vs the x coordinate; b) Electron trajectories in the (x, p_x, p_z) space. Inset shows zoomed trajectory for $x(0) = 0.2$ corresponding to a strange attractor [27]. c) Electron gamma-factor γ_e versus the coordinate x . Inset shows zoomed $\gamma_e(x)$ for $x(0) = 0.2$ d) Parameter χ_e versus the coordinate x , for the same initial conditions.

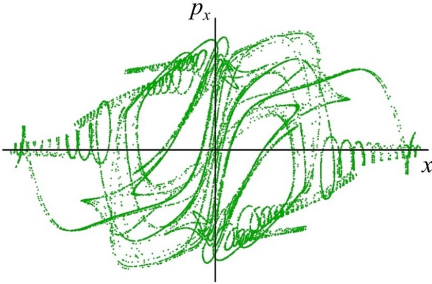


FIG. 9. The Poincaré sections showing the particle positions in the phase plane (x, p_x) at discrete times with the time step equal to the period of the driving force. The parameters are the same as in Fig. 8 for $x(0) = 0.49$.

We also assume that the time average of the function $\xi(t)$ over the oscillation period $2\pi/\omega$ is zero. Introducing the notation

$$\langle x \rangle = \frac{\omega}{2\pi} \int_0^{2\pi/\omega} x(t) dt, \quad (34)$$

we obtain

$$\langle \xi \rangle = \langle \dot{\xi} \rangle = \langle \ddot{\xi} \rangle = 0. \quad (35)$$

Therefore, we have $\langle x \rangle = X(t)$, i.e. the function $X(t)$ describes the slow particle motion averaged over the fast oscillations, $\langle X \rangle \approx X(t)$.

Substituting (33) into the equation of particle motion (31) and expanding the functions $\kappa(x, t)$ and $F(x, t)$ in powers of ξ , i. e. writing $\kappa(x, t) \approx \kappa(X, t) + \xi \partial_X \kappa(X, t)$ and $F(x, t) \approx F(X, t) + \xi \partial_X F(X, t)$, we obtain

$$\ddot{X} + \ddot{\xi} + \kappa \dot{X} + \kappa \dot{\xi} + \xi \dot{X} \partial_X \kappa + \xi \dot{\xi} \partial_X \kappa = F + \xi \partial_X F, \quad (36)$$

where ∂_X is the partial derivative with respect to the first argument of functions $\kappa(X, t)$ and $F(X, t)$. This equation contains slowly varying and fast oscillating terms, which apparently should be separately equal to each other. In the zeroth order approximation with respect to small function ξ and the time derivatives of the slow function X , we find the equation for the fast oscillating term

$$\ddot{\xi} + \kappa \dot{\xi} = F. \quad (37)$$

Here we neglect the terms proportional to ξ . The time derivatives $\dot{\xi}$ and $\ddot{\xi}$ are not small, being proportional to ω^2 and ω , respectively. They are assumed to be much greater than \dot{X} and \ddot{X} . The friction coefficient κ is not necessarily small.

Integration of Eq. (37), assuming X to be constant,

yields

$$\xi = \xi_0 + \int_0^t d\tau \left[e^{-K(X,\tau)} \dot{\xi}_0 + \int_0^\tau e^{K(X,\tau') - K(X,\tau)} F(X,\tau') d\tau' \right], \quad (38)$$

$$K(X, t) = \int_0^t \kappa(X, \tau) d\tau. \quad (39)$$

Assuming that $K(X, t)$ can be approximated by $K(X, t) \approx \langle \kappa \rangle t$, where $\langle \kappa \rangle$ is the time-averaged friction coefficient, in the limit $t \gg 1/\langle \kappa \rangle$ we obtain

$$\begin{aligned} \xi &= \frac{(\langle \kappa \rangle f_1 - \omega f_2) \sin \omega t - (\langle \kappa \rangle f_1 + \omega f_2) \cos \omega t}{\omega(\langle \kappa \rangle^2 + \omega^2)} \\ &= -\frac{1}{\langle \kappa \rangle^2 + \omega^2} \left(F + \frac{\langle \kappa \rangle}{\omega^2} \partial_t F \right) \end{aligned} \quad (40)$$

with $\partial_t F = \partial F(X, t)/\partial t|_{X=\text{const}}$. Here we assumed the initial condition $\xi_0 = -(f_2 + \omega \xi_0)/(\langle \kappa \rangle \omega)$.

Averaging Eq. (36) over time and taking into account that $\langle F(X, t) \rangle \approx 0$ for nearly constant $X(t)$, we obtain

$$\ddot{X} + (\langle \kappa \rangle + \langle \xi \partial_X \kappa \rangle) \dot{X} = \langle \xi \partial_X F \rangle - \langle \xi \dot{\xi} \partial_X \kappa \rangle. \quad (41)$$

Substituting expression (40) into the r.h.s. of Eq. (41), for the first term we obtain

$$\langle \xi \partial_X F \rangle = -\frac{\partial_X(f_1^2 + f_2^2)}{4(\langle \kappa \rangle^2 + \omega^2)} - \frac{\langle \kappa \rangle (f_2 \partial_X f_1 - f_1 \partial_X f_2)}{2\omega(\langle \kappa \rangle^2 + \omega^2)}. \quad (42)$$

The first term on the r.h.s. of Eq. (42) is the well known ponderomotive force [88] where the friction effect is taken into account. The last term on the r.h.s., proportional to the friction coefficient, can change signs for $f_2 \partial_X f_1 \neq f_1 \partial_X f_2$ depending on whether $f_2 \partial_X f_1 > f_1 \partial_X f_2$ or $f_2 \partial_X f_1 < f_1 \partial_X f_2$. It vanishes if $f_2 \partial_X f_1 = f_1 \partial_X f_2$, $f_1 \neq 0$, $f_2 = 0$ or $f_2 \neq 0$, $f_1 = 0$.

The actual form of the last term on the r.h.s. of Eq. (41) is determined by the specific dependence of the friction coefficient κ on the driver force. As an example, we consider the case when this dependence is quadratic, i.e. $\kappa = \nu F^2$, with a constant ν . Then we obtain

$$\begin{aligned} -\langle \xi \dot{\xi} \partial_X \kappa \rangle &= \frac{\nu \langle \kappa \rangle \partial_X (f_1^2 + f_2^2)^2}{8(\langle \kappa \rangle^2 + \omega^2)^2} + \\ &\frac{\nu(\langle \kappa \rangle^2 - \omega^2)(f_1^2 + f_2^2)(f_2 \partial_X f_1 - f_1 \partial_X f_2)}{4\omega(\langle \kappa \rangle^2 + \omega^2)^2} \end{aligned} \quad (43)$$

and the time-averaged friction coefficient becomes $\langle \kappa \rangle = \nu(f_1^2 + f_2^2)/2$. In addition, $\langle \xi \partial_X \kappa \rangle = 0$.

For the sake of simplicity we further assume that $f_2 = 0$ in expression (32) for the driver force. Then, Eqs. (42) and (43) are simplified and we finally obtain the equation for the slowly varying function $X(t)$:

$$\ddot{X} + \frac{\nu f_1^2}{2} \dot{X} = -\frac{\partial_X f_1^2}{\nu^2 f_1^4 + 4\omega^2} + \frac{2\nu^2 \partial_X f_1^6}{3(\nu^2 f_1^4 + 4\omega^2)^2}. \quad (44)$$

The first term on the r.h.s. corresponds to the ponderomotive force, the last term is the drag force induced by the friction.

As we can see, the ponderomotive force (42) and the drag force due to the friction (43) have different signs in Eq. (44). If

$$|\nu| > 2\omega/f_1^2, \quad (45)$$

the drag force exceeds in magnitude the ponderomotive force. Using Eq. (22) for radiation friction force and the equation (18) of electron motion we can find that the criterion (45) can be written as the condition on the laser amplitude, $a \varepsilon_{rad}^{1/3} > 1$, i.e. the drag force due to the radiation friction is larger than the ponderomotive force in the radiation friction dominated regime (see Ref. [87]).

Numerical integration of the equation of motion (31) with

$$F(x, t) = f_0 \exp(-(x/l_0)^2) \cos \omega t \quad \text{and} \quad \kappa = \nu F^2 \quad (46)$$

reveals the main features of the behavior predicted within the framework of the simple model approximation. The solutions for the cases of relatively weak and relatively strong driver force are plotted in Fig. 10. The parameters are as follows. The driver frequency and the friction coefficient values are $\omega = 1$ and $\nu = 0.1$, respectively. The driver width equals $l_0 = 5$. The initial coordinate and velocity are $x_0 = 3$ and $\dot{x}_0 = 1$, in both cases. The driver amplitude is equal to $f_0 = 5\sqrt{2\omega/\nu}$ in the case of the weak driver, and is equal to $f_0 = 15\sqrt{2\omega/\nu}$ in the case of the strong driver. As we see in Fig. 10 a) and b), in the case of weak nonlinearity, the particle being pushed outwards by the ponderomotive force having performed several oscillations leaves the region where the driver force is localized. In contrast, in the limit of strong nonlinearity, the friction drag force prevents the particle from leaving the driver localization region resulting in its slow drift inwards (Fig. 10 c) and d)).

On a trajectory corresponding to a quasi-periodic particle motion seen in Fig. 10, the particle feels an almost constant driving force. This situation can be described in the approximation

$$F(x, t) = f_0 \cos \omega t, \quad \kappa = \nu f_0^2 \cos^2 \omega t. \quad (47)$$

Substituting this driving force and friction coefficient into Eq. (31), we change variables to $(\tau, y(\tau))$, $t = \tau/\omega$, $x(t) = (f_0/\omega^2)y(\tau)$ and introduce the constant

$$\sigma = \nu f_0^2/\omega. \quad (48)$$

Thus, we obtain

$$y''(\tau) + \sigma \cos^2(\tau) y'(\tau) = \cos \tau. \quad (49)$$

Here a prime denotes a differentiation with respect to the variable τ . Using Eq. (39) and the generating function

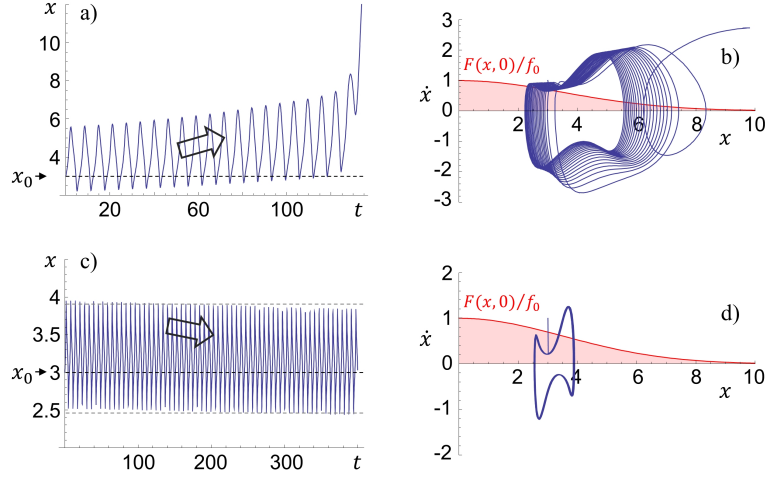


FIG. 10. The solutions of Eq. (31) in the case of relatively weak driver force (a and b), and for the case of relatively strong driver force (c and d). a) and c) Dependence of the particle coordinate on time. b) and d) The particle trajectory in the phase plane (x, \dot{x}) .

for the modified Bessel functions of the first kind, I_k , one can cast the general solution to Eq. (49) in the form

$$y'(\tau) = \exp\left(-\frac{\sigma\tau}{2} - \frac{\sigma}{4}\sin(2\tau)\right) [y'(0) - Y_{LC}(0)] + Y_{LC}(\tau), \quad (50)$$

where the function $Y_{LC}(\tau)$ is given by

$$Y_{LC}(\tau) = \exp\left(-\frac{\sigma}{4}\sin(2\tau)\right) \sum_{k=-\infty}^{\infty} (-i)^{k+1} I_k\left(\frac{\sigma}{4}\right) \times \left\{ \frac{\exp[i(2k-1)\tau]}{4k-2-i\sigma} + \frac{\exp[i(2k+1)\tau]}{4k+2-i\sigma} \right\}. \quad (51)$$

As one can see, any solution at $\tau \rightarrow \infty$ tends to the limit cycle described by the function Y_{LC} and determined by the constant $y'(0) = Y_{LC}(0)$.

The function describing the limit cycle, Eq. (51), can be represented as a Fourier series in terms of odd harmonics of the driving force frequency

$$Y_{LC}(\tau) = \sum_{n=1}^{\infty} [\exp(i(2n-1)\tau) C_n(\sigma) + \exp(-i(2n-1)\tau) C_{1-n}(\sigma)] \quad (52)$$

with

$$C_n(\sigma) = i^n \sum_{k=-\infty}^{\infty} \frac{(-1)^{k+1}}{4k+2-i\sigma} [I_k\left(\frac{\sigma}{4}\right) - iI_{k+1}\left(\frac{\sigma}{4}\right)] I_{k+1-n}\left(\frac{\sigma}{4}\right). \quad (53)$$

This gives the spectrum of the limit cycle trajectory. For the particle velocity (corresponding to $y'(\tau)$), the spectral density is $|2C_n(\sigma)|^2$, Fig. 11.

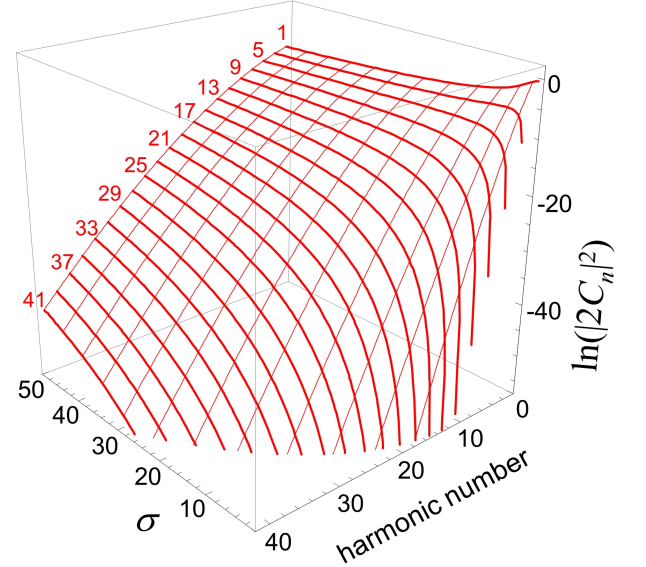


FIG. 11. The spectral density of the particle velocity for several harmonics of the driving force frequency as a function of the friction parameter σ .

V. REGULAR AND CHAOTIC ELECTRON MOTION IN THREE S- AND P-POLARIZED COLLIDING LASER PULSES

A. EM field configuration

Let us consider three s(p)-polarized waves, which z -component of the electric (magnetic) field is given by

$$\begin{pmatrix} E_z \\ B_z \end{pmatrix} = -\frac{1}{\sqrt{3}} \begin{pmatrix} E_0 \\ B_0 \end{pmatrix} \left\{ \sin \left[\omega_0 \left(t + \frac{y}{c} \right) \right] \right\}$$

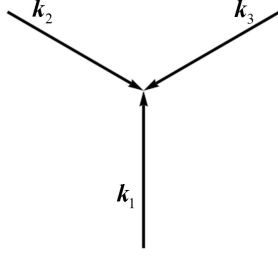


FIG. 12. Wave vectors of three colliding waves.

$$+2 \sin \left[\omega_0 \left(t - \frac{y}{2c} \right) \right] \cos \left(\omega_0 \frac{\sqrt{3}x}{2c} \right) \Bigg\}. \quad (54)$$

The x and y components of the magnetic (electric) field of the s(p)-polarized wave are

$$\begin{aligned} \begin{pmatrix} B_x \\ E_x \end{pmatrix} &= \frac{1}{\sqrt{3}} \begin{pmatrix} E_0 \\ -B_0 \end{pmatrix} \left\{ -\sin \left[\omega_0 \left(t + \frac{y}{c} \right) \right] \right. \\ &\quad \left. + \sin \left[\omega_0 \left(t - \frac{y}{2c} \right) \right] \cos \left(\omega_0 \frac{\sqrt{3}x}{2c} \right) \right\} \end{aligned} \quad (55)$$

and

$$\begin{pmatrix} B_y \\ E_y \end{pmatrix} = \frac{1}{\sqrt{3}} \begin{pmatrix} E_0 \\ -B_0 \end{pmatrix} \cos \left[\omega_0 \left(t - \frac{y}{2c} \right) \right] \sin \left(\omega_0 \frac{\sqrt{3}x}{2c} \right). \quad (56)$$

The wave orientation is illustrated in Fig. 12. As an example in Fig. 13 a) we show the magnetic (electric) field $\mathbf{B}_n = B_x \mathbf{e}_x + B_y \mathbf{e}_y$ ($\mathbf{E}_n = E_x \mathbf{e}_x + E_y \mathbf{e}_y$) and in Fig. 13 b) the isocontours of the electric (magnetic) field E_z (B_z) in the (x, y) plane at time $t = \pi/4$ for the case of three colliding s-polarized (p-polarized) EM waves.

B. Electron interaction with three s-polarized EM waves

1. Particular solutions

Due to the symmetry of the EM field given by Eqs. (55, 56), there are particular solutions of the equations of motion, when the particle moves straight in the (x, y) plane along the direction of one of the waves propagation. If we let $x = 0$ in Eqs. (55, 56), the electromagnetic field formally corresponds to a superposition of two EM waves one of which propagates with the velocity equal to $-c$ and another has the velocity $2c$.

The integration of the equations of electron motion yields the particle trajectories presented in Fig. 14 for initial conditions: $x(0) = 0, y(0) = 0.05, z(0) = 0, p_x(0) = 0, p_y(0) = 0, p_z(0) = 0$. The normalized electromagnetic field amplitude is $a_0 = 436$ (each of the colliding waves

has the amplitude equal to $a_0/3$), the dissipation parameter is $\varepsilon_{rad} = 1.2 \times 10^{-8}$, and the normalized critical QED field is $a_S = 4 \times 10^5$. The electron trajectory in the (y, z) plane plotted in Fig. 14 a) and the trajectory in the phase (y, p_z) plane shown in Fig. 14 b) look similar to the trajectories presented in Fig. 2 a) and b). The particle is trapped for a finite time within the EM field period performing relatively small scale oscillations. Then after some time it over-leaps to the next EM field period. This is also clearly seen in Fig. 14 c), where its y -coordinate is plotted versus time. From the Poincaré sections in Fig. 14 d), which show the particle positions in the phase plane (p_z, p_y) at discrete times with the time step equal to the period of the driving force, we may see that this process is stochastic. The particle over-leaping from one field period to another with small scale oscillations in between (see Figs. 2, 3 and 14) may be interpreted in terms of Lévy flights [82–85].

The case of high laser amplitude is presented in Fig. 15 for initial conditions: $x(0) = 0, y(0) = -0.0001, z(0) = 0, p_x(0) = 0, p_y(0) = 0, p_z(0) = 0$. The normalized electromagnetic field amplitude is $a_0 = 4700$ (each of the colliding waves has the amplitude equal to $a_0/3$), the dissipation parameter is $\varepsilon_{rad} = 1.2 \times 10^{-9}$, and the normalized critical QED field is $a_S = 4 \times 10^6$. The electron trajectory in the (y, z) plane plotted in Fig. 15 a) and the trajectory in the phase (y, p_y) plane shown in Fig. 15 b) clearly demonstrate the particle trapping into the limit circle after an initial phase corresponding to the particle motion in the vicinity of the electric field node, $y = 0$. Since the motion here is unstable, the particle leaves this region. This is also distinctly seen in Fig. 15 d) showing the electron trajectory in the (p_y, p_z) plane. In the plane (y, z) (Fig. 15 a)) as we see, when particle moves along the limit circle, its trajectory has the “figure eight” form. It performs regular oscillations (see Fig. 15 c), where the particle coordinate y is plotted versus time) with the double frequency for oscillations along the y axis compared with the frequency of oscillation along the z axis.

2. Random-walk and regular patterns of the particle trajectories in the field of three 3 s-polarized EM waves

Results of integrations of the motion equations for the electron interacting with three 3 s-polarized EM waves in the limit of relatively low radiation intensity are presented in Fig. 16. Fig. 16 a) shows 8 electron trajectories in the (x, y) plane for initial conditions: $x(0)$ and $y(0)$ are in the vicinity of the coordinate origin, and $z(0) = 0, p_x(0) = 0, p_y(0) = 0, p_z(0) = 0$. In Fig. 16 b) we plot a close up of the trajectories in the vicinity of the coordinate origin superimposed with the isocontours of the electromagnetic potential averaged over a half period of the field oscillations. It is proportional to the ponderomotive potential in the high field amplitude limit, $a_0 \gg 1$. As we see the typical trajectories are comprised of long range Lévy-flight-like excursions and

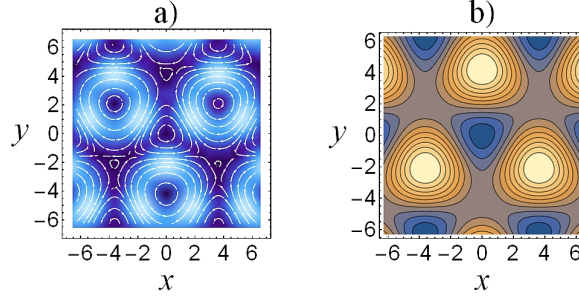


FIG. 13. Three s-polarized (p-polarized) EM waves: a) magnetic (electric) field; b) isocontours of the electric (magnetic) field in the (x, y) plane at time $t = \pi/4$.

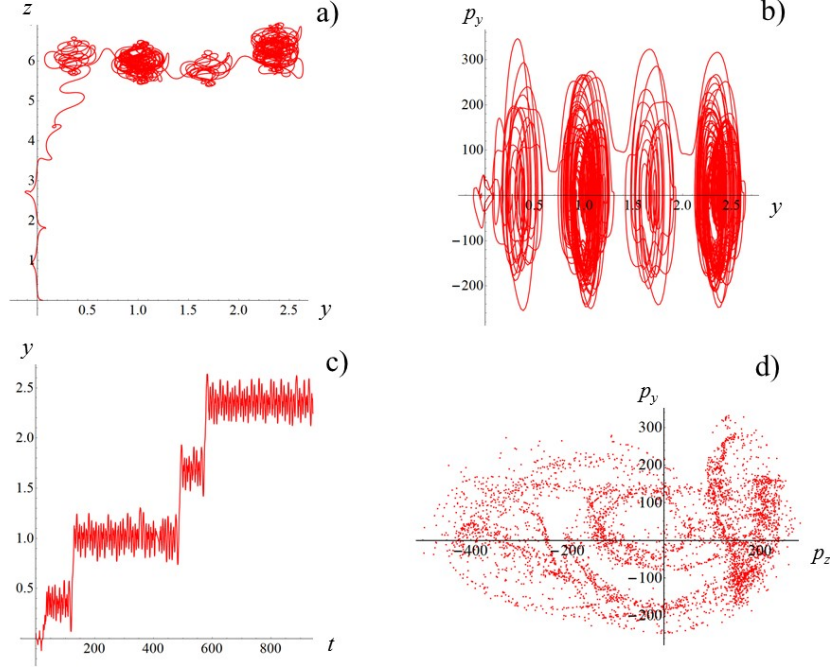


FIG. 14. a) Electron trajectory in the (y, z) plane for initial conditions: $x(0) = 0, y(0) = 0.05, z(0) = 0, p_x(0) = 0, p_y(0) = 0, p_z(0) = 0$. b) Trajectory in the phase (y, p_y) plane; c) Electron y -coordinate versus time; d) The Poincaré sections showing the particle positions in the phase plane (p_z, p_y) at discrete times with the time step equal to the period of the driving force. The electromagnetic field amplitude is $a_0 = 436$, the dissipation parameter is $\varepsilon_{rad} = 1.2 \times 10^{-8}$, and the normalized critical QED field is $a_S = 4 \times 10^5$. The coordinates, time and momentum are measured in the $2\pi c/\omega, 2\pi/\omega$ and $m_e c$ units.

short range rambling motion, which changes the direction of succeeding flight. The combination of the long range excursions and short range rambling is also seen in the dependence of the electron y coordinate on time in Fig. 16 d). The corresponding particle trajectory in the p_x, p_y, p_z momentum space for $x(0) = -0.125$ and $y(0) = 0.125$ is presented in Fig. 16 c). What is remarkable is that during the Lévy-like flights the electron moves almost along the direction of one of the three waves propagation (compare Figs. 12 and Fig. 16 a)). This stage of the particle motion can be described by the particular solution analyzed above and illustrated in Fig. 14.

Qualitatively different patterns formed by the trajec-

tories of particles interacting with the field of three 3 s-polarized EM waves are observed in the high intensity and low frequency limit. These patterns are shown in Fig. 17 a) and in Fig. 17 b) presenting a close up of the trajectories in the vicinity of the coordinate origin, where the trajectories in the (x, y) plane of an electron ensemble make a tracery striking the imagination reminding one of a parquetry or window frost. Either an individual trajectory or their ensemble appear to be confined in the lower measure sub-domain periodic in the x and y directions. In Fig. 17 c) the electron trajectory in the p_x, p_y, p_z momentum space for $x(0) = -0.125$ and $y(0) = 0.125$ demonstrates that the particle energy re-

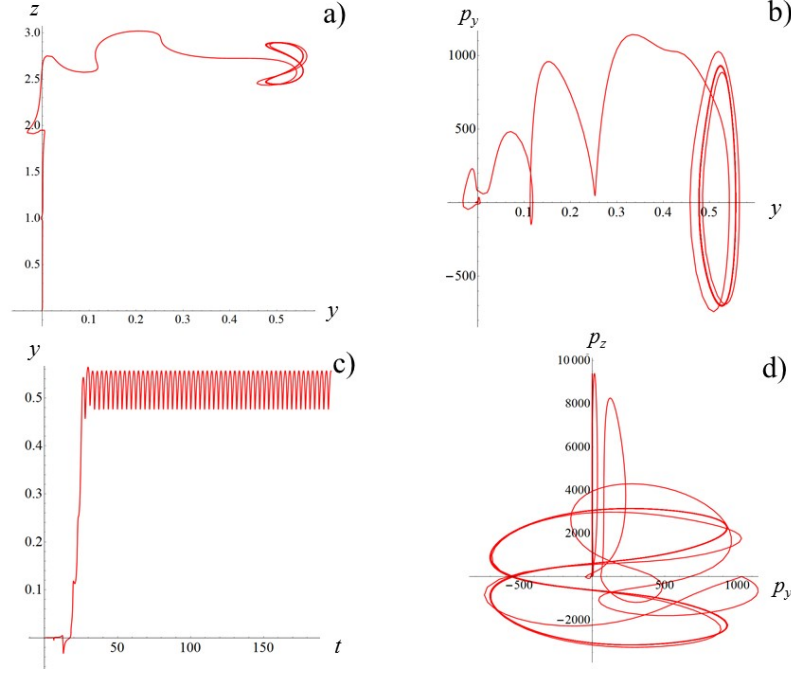


FIG. 15. a) Electron trajectory in the (y, z) plane for initial conditions: $x(0) = 0, y(0) = -0.0001, z(0) = 0, p_x(0) = 0, p_y(0) = 0, p_z(0) = 0$. b) Trajectory in the phase plane (y, p_y) ; c) Electron y -coordinate versus time; d) Electron trajectory in the (p_y, p_z) plane. The electromagnetic field amplitude is $a_0 = 4700$, the dissipation parameter is $\varepsilon_{rad} = 1.2 \times 10^{-9}$, and the normalized critical QED field is $a_S = 4 \times 10^6$. The coordinates, time and momentum are measured in the $2\pi c/\omega$, $2\pi/\omega$ and $m_e c$ units.

mains finite. The electron y coordinate dependence on time for $x(0) = -0.001$ and $y(0) = -0.001$ plotted in Fig. 17 c) shows that the particle motion is comprised of relatively long over-leaps interlaced with small-scale oscillations. In Fig. 17 e) we present the corresponding Poincaré sections, i. e. we plot the particle positions in the phase plane (p_x, p_y) at discrete times with the time step equal to the period of the driving force. The Poincaré sections, in this case, indicate that the particle motion is pretty regular. Here the parameters of the EM field and of the electrons are as follows. The electromagnetic field amplitude is $a_0 = 4764$ (the amplitude of each colliding waves is equal to 1588), the dissipation parameter is $\varepsilon_{rad} = 6 \times 10^{-9}$, and the normalized critical QED field is $a_S = 8 \times 10^5$, which corresponds to the wave frequency a factor two smaller than in the case shown in Fig. 16. The integration time equals $200 \times 2\pi/\omega$

3. Ergodization or not?

The attractor trajectory pattern in Fig. 17 a) and b) is made by an ensemble of electrons. The single electron trajectory shown in Fig. 18 demonstrates that having been moving for a long enough time it could cover the whole attractor. In view of this, there are two questions. The first one being is there an analogy of the ergodic hy-

pothesis saying that over long periods of time, the time spent in some region of the attractor is proportional to the attractor measure? The second one being is there an analogy of the Poincaré recurrence theorem [89] saying that the particle, after a sufficiently long but finite time, returns to a point very close to the initial point? A similar question occurs in the case of the particle random walk on whether the results of well known random walk theory [90] can be used in our case.

C. Electron interaction with three p-polarized EM waves

In the case of three p-polarized EM waves the EM configuration is described by Eqs. (54), (55), (56). As in the s-polarization case, in the limit of relatively low EM wave intensity the electron performs the random walk motion comprised of short scale-length oscillations interleaved by long scale-length Lévy-like flights. An example of such the trajectory is shown in Fig. 19 a) for the EM field amplitude of $a_0 = 4764$, the dissipation parameter of $\varepsilon_{rad} = 6 \times 10^{-9}$, and the normalized critical QED field of $a_S = 8 \times 10^5$. For the high intensity EM wave case the electrons migrate along the paths confined in narrow valleys as can be seen in Fig. 19 b), where the ensemble of the electron trajectories is plotted for the EM

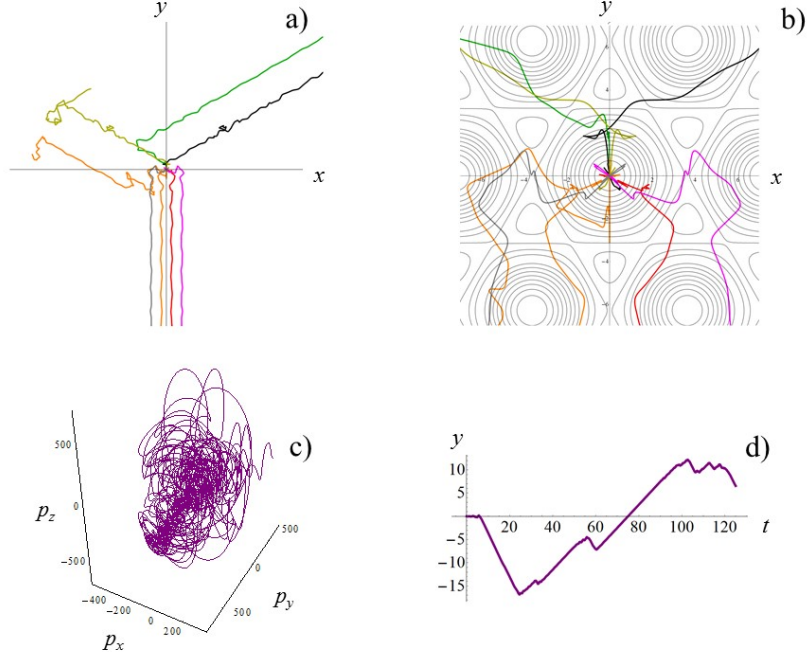


FIG. 16. a) 8 electron trajectories in the (x, y) plane for initial conditions: $x(0)$ and $y(0)$ are in the vicinity of the coordinate origin, and $z(0) = 0$, $p_x(0) = 0$, $p_y(0) = 0$, $p_z(0) = 0$. b) Close up of the trajectories in the vicinity of the coordinate origin. c) Electron trajectory in the p_x, p_y, p_z space for $x(0) = -0.125$ and $y(0) = 0.125$. d) Electron y coordinate versus time for $x(0) = -0.125$ and $y(0) = 0.125$. The electromagnetic field amplitude is $a_0 = 756$, the dissipation parameter is $\varepsilon_{rad} = 1.2 \times 10^{-8}$, and the normalized critical QED field is $a_S = 4 \times 10^5$. The coordinates, time and momentum are measured in the $2\pi c/\omega$, $2\pi/\omega$ and $m_e c$ units.

field amplitude of 7.2×10^3 , the dissipation parameter of $\varepsilon_{rad} = 1.2 \times 10^{-8}$, and the normalized critical QED field of $a_S = 4.1 \times 10^5$.

VI. ELECTRON DYNAMICS IN FOUR S- AND P-POLARIZED COLLIDING EM PULSES

The orientation of four colliding waves is illustrated in Fig. 20. Fig. 21 a) shows magnetic (electric) field and b) isocontours of the electric (magnetic) field in the (x, y) plane at time $t = \pi/4$ of four s-polarized (p-polarized) colliding EM waves.

A. S-polarized 4 colliding EM waves

B. EM field configuration

In the EM configuration of four colliding s(p)-polarized waves the z -components of the electric (magnetic) field can be written

$$\begin{pmatrix} E_z \\ B_z \end{pmatrix} = \begin{pmatrix} E_0 \\ B_0 \end{pmatrix} 2 \sin(\omega_0 t) \left[\cos\left(\omega_0 \frac{x}{c}\right) + \cos\left(\omega_0 \frac{y}{c}\right) \right]. \quad (57)$$

The x and y components of the magnetic (electric) field of the four colliding s(p)-polarized waves are given by

$$\begin{pmatrix} B_x \\ E_x \end{pmatrix} = \begin{pmatrix} -E_0 \\ B_0 \end{pmatrix} 2 \cos(\omega_0 t) \sin\left(\omega_0 \frac{y}{c}\right) \quad (58)$$

and

$$\begin{pmatrix} B_y \\ E_y \end{pmatrix} = \begin{pmatrix} E_0 \\ -B_0 \end{pmatrix} 2 \cos(\omega_0 t) \sin\left(\omega_0 \frac{x}{c}\right), \quad (59)$$

respectively.

1. Particular solutions

As in the above considered case of three s-polarized EM waves the equations of electron motion admit particular solutions, in the first of which the particle moves either along one of the axis, i.e. $x = nc\pi/\omega$ or $y = nc\pi/\omega$ with $n = 0, \pm 1, \pm 2, \dots$, and in the second it moves along straight lines $x = \pm y + nc\pi/\omega$.

First type solution. For the first class of particular solutions with $x = nc\pi/\omega$ (without loss of generality we may take $n = 0$, i. e. consider $x = 0$), formally the particle moves in a superposition of the fields of two counter-propagating s-polarized EM waves and a homogeneous oscillating electric field directed along the z axis. As in

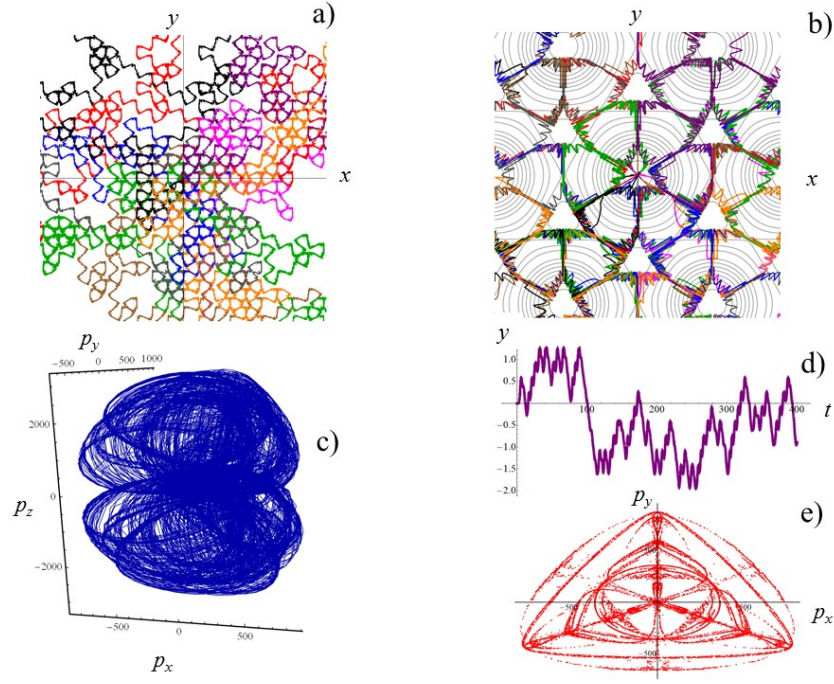


FIG. 17. a) Ensemble of electron trajectories in the (x, y) plane for initial conditions: $x(0)$ and $y(0)$ are in the vicinity of the coordinate origin, and $z(0) = 0$, $p_x(0) = 0$, $p_y(0) = 0$, $p_z(0) = 0$. b) Close up of the trajectories in the vicinity of the coordinate origin. c) Electron trajectory in the p_x, p_y, p_z space for $x(0) = -0.125$ and $y(0) = 0.125$. d) Electron y coordinate versus time for $x(0) = -0.001$ and $y(0) = -0.001$. e) The Poincaré sections: the particle positions in the phase plane (p_x, p_y) at discrete times with the time step equal to the period of the driving force. The electromagnetic field amplitude is $a_0 = 4764$, the dissipation parameter is $\varepsilon_{rad} = 6 \times 10^{-9}$, and the normalized critical QED field is $a_S = 8 \times 10^5$. The coordinates, time and momentum are measured in the $2\pi c/\omega$, $2\pi/\omega$ and $m_e c$ units. The integration time equals $200 \times 2\pi/\omega$.

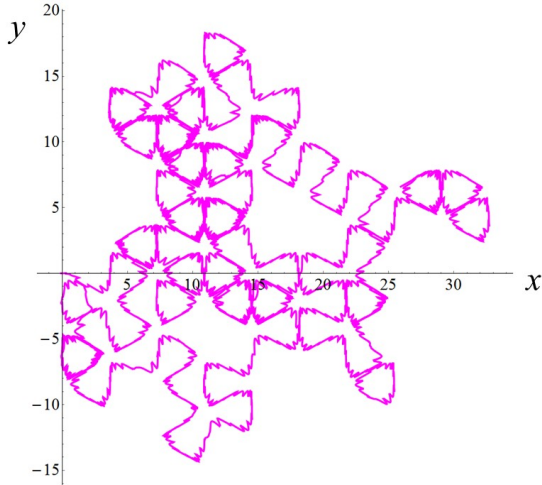


FIG. 18. Trajectory of the electron migrating over a long time in the (x, y) plane.

the above considered cases of two and three colliding EM waves, in the limit of weak nonlinearity and dissipation ($\varepsilon_{rad} = 1.2 \times 10^{-9}$, $a_S = 4 \times 10^6$, $a = 94$, $\omega = 0.1$, for ini-

tial conditions: $y(0) = 0.01$, $z(0) = 0$, $p_x(0) = 0$, $p_z(0) = 0$ (red,-1); $y(0) = 0.23$, $z(0) = 0$, $p_x(0) = 0$, $p_z(0) = 0$ (blue,-2); $y(0) = 0.45$, $z(0) = 0$, $p_x(0) = 0$, $p_z(0) = 0$ (green,-3)) the particle motion can be described as a random walk, for which the trajectories consist of the relatively small amplitude fast oscillating parts and of the long scale length Lévy flights (see Fig. 22 a) and b)). The Poincaré sections, the particle positions in the phase plane (p_y, p_z) at discrete times with the time step equal to the period of the driving force, presented in Fig. 22 c) show that the electron motion is stochastic.

In the case of lower frequency, $\omega = 0.02$, and higher dimensionless EM field amplitude $a = 8 \times 10^3$, when $\varepsilon_{rad} = 2.4 \times 10^{-10}$, $a_S = 2 \times 10^7$, $a_0 = 8 \times 10^3$, $\omega = 0.02$, the electron trajectories in the (y, z) plane (see Fig. 22 d)) show that the particles are trapped within narrow regions moving along regular limit circles (Fig. 22 e)). The attractor geometry is distinctly seen in Fig. 22 f), where the trajectories in the (y, p_y, p_z) space are presented. As well seen, after a relatively short initial time interval the particles are trapped into stable limit circles performing periodic motion. We note that for the parameters chosen although the particle energy is ultrarelativistic the value of χ_e remains below unity, i.e. the QED effect of the recoil is not significant.

Second type solution. The particle behavior under

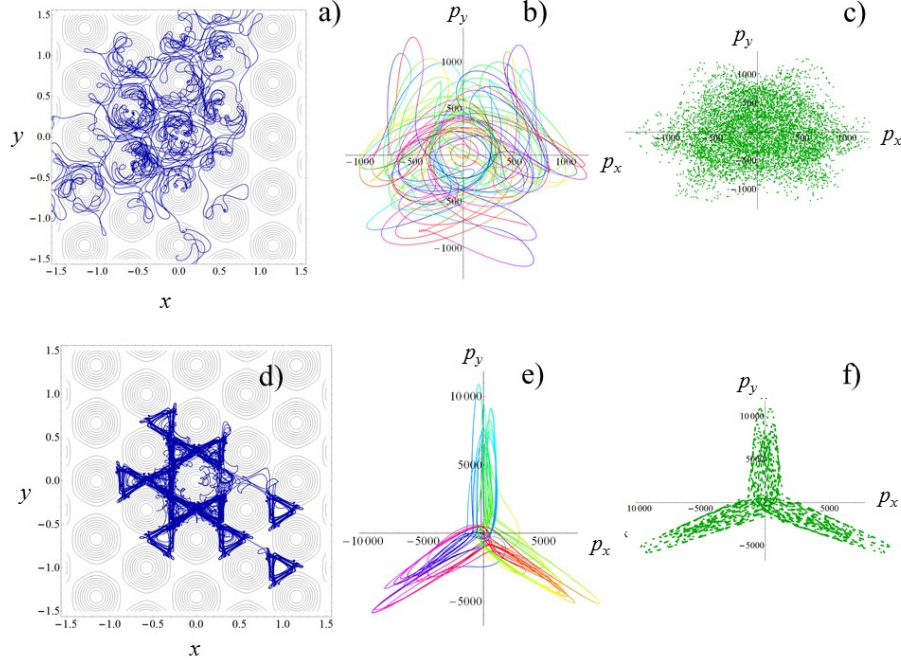


FIG. 19. a) Ensemble of electron trajectories in the (x, y) plane for initial conditions: $x(0)$ and $y(0)$ are in the vicinity of the coordinate origin, and $z(0) = 0$, $p_x(0) = 0$, $p_y(0) = 0$, $p_z(0) = 0$. b) Electron trajectories in the (p_x, p_y) plane. c) The Poincaré sections: the particle positions in the phase plane (p_x, p_y) at discrete times with the time step equal to the period of the driving force. The electromagnetic field amplitude is $a_0 = 1383$, the dissipation parameter is $\varepsilon_{rad} = 1.2 \times 10^{-6}$, and the normalized critical QED field is $a_S = 4.1 \times 10^5$. d) Ensemble of electron trajectories in the (x, y) plane for initial conditions: $x(0)$ and $y(0)$ are in the vicinity of the coordinate origin, and $z(0) = 0$, $p_x(0) = 0$, $p_y(0) = 0$, $p_z(0) = 0$. e) Electron trajectories in the (p_x, p_y) plane. f) The Poincaré sections: the particle positions in the phase plane (p_x, p_y) at discrete times with the time step equal to the period of the driving force. The electromagnetic field amplitude is $a_0 = 7.2 \times 10^3$, the dissipation parameter is $\varepsilon_{rad} = 1.2 \times 10^{-8}$, and the normalized critical QED field is $a_S = 4.1 \times 10^5$.

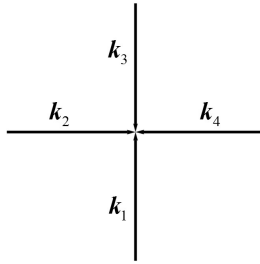


FIG. 20. Wave vectors of four colliding EM waves.

the conditions corresponding to the second class of particular solutions of the equations of motion ($x = y$) is illustrated in Figs. 23 and 24. Here the coordinate $s(t)$ is equal to $s = x = y$.

In Fig. 23 we present electron trajectories in the case corresponding to the motion along the $x = y$ direction in the field of four colliding EM waves for $\varepsilon_{rad} = 1.2 \times 10^{-8}$, $a_S = 4 \times 10^5$, $a_0 = 44$, $\omega = 1$ for initial conditions: $x(0) = 0.01$, $z(0) = 0$, $p_x(0) = 0$, $p_z(0) = 0$ (red,-1); $x(0) = 0.23$, $z(0) = 0$, $p_x(0) = 0$, $p_z(0) = 0$ (blue,-2); $x(0) = 0.45$, $z(0) = 0$, $p_x(0) = 0$, $p_z(0) = 0$ (green,-

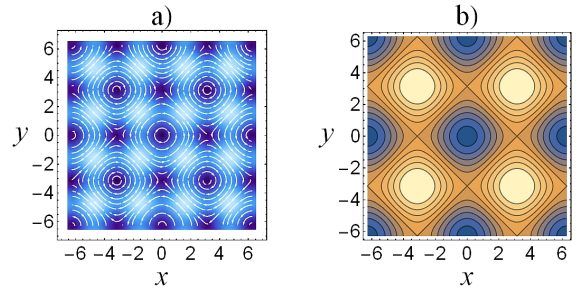


FIG. 21. Four s-polarized (p-polarized) EM waves: a) magnetic (electric) field; b) isocontours of the electric (magnetic) field in the (x, y) plane at time $t = \pi/4$.

3). Fig. 23 a) shows electron trajectories in the (s, z) plane, which demonstrate random walks with intermittent short scale length oscillations and long range Lévy flights. The same behavior is distinctly seen in Fig. 23 b) with three dependences of the s coordinates on time. Stochastic character of the particle motion is demonstrated in Figs. 23 b) and f) by the behavior of trajectories in the (s, p_s, p_z) space and by the particle po-

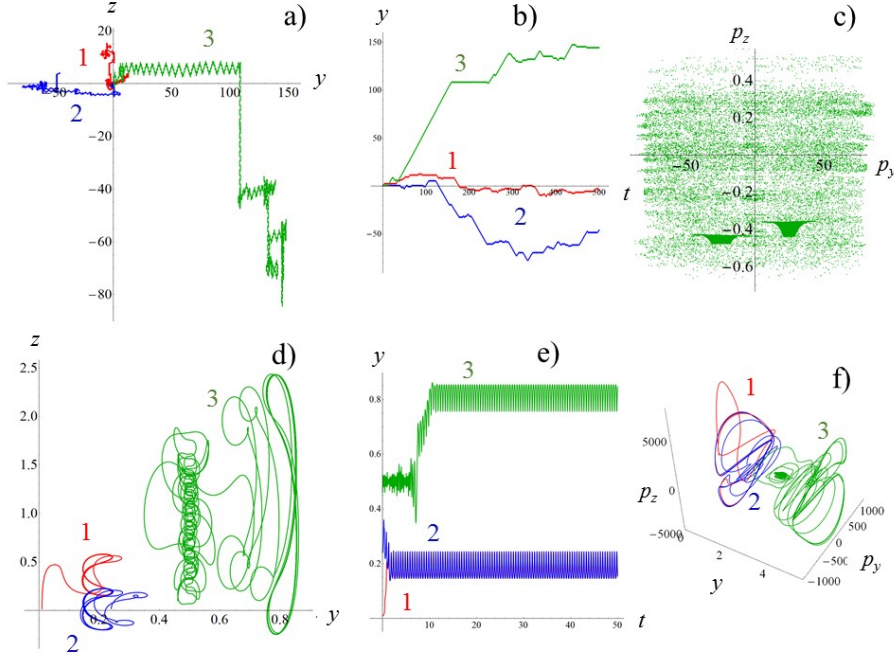


FIG. 22. Electron trajectories in the case of **the first type** particular solution corresponding to the motion along the y axis (at $x = 0$) in the field of four colliding EM waves for $\varepsilon_{rad} = 1.2 \times 10^{-9}$, $a_S = 4 \times 10^6$, $a = 94$, $\omega = 0.1$ for initial conditions: $y(0) = 0.01$, $z(0) = 0$, $p_y(0) = 0$, $p_z(0) = 0$ (red,-1); $y(0) = 0.23$, $z(0) = 0$, $p_y(0) = 0$, $p_z(0) = 0$ (blue,-2); $y(0) = 0.45$, $z(0) = 0$, $p_x(0) = 0$, $p_z(0) = 0$ (green,-3). a) Trajectories in the (y, z) plane. b) Dependences of the y coordinates on time. c) The Poincaré sections: the particle positions in the phase plane (p_y, p_z) at discrete times with the time step equal to the period of the driving force. For lower frequency, $\omega = 0.02$, when $\varepsilon_{rad} = 2.4 \times 10^{-10}$, $a_S = 2 \times 10^7$, $a_0 = 8 \times 10^3$, they are shown d) trajectories in the (y, z) plane, e) dependences of the y coordinates on time, and f) trajectories in the (y, p_y, p_z) space for the same initial conditions as in the frames a,b,c).

sitions in the phase plane (p_s, p_z) at discrete times with the time step equal to the period of the driving force, respectively. According to Fig. 23 d), where the particle Lorentz factor γ is plotted versus time, the normalized electron energy is of the order of the dimensionless EM field amplitude, i. e. $\gamma \approx a_0$. From the dependence of the parameter χ on time in Fig. 23 e) it follows that, in this case, the QED effect of the recoil is not significant.

The electron interaction with four colliding EM waves in the case of **the second type** particular solution corresponding to the motion along the $x = y$ direction is illustrated in Fig. 24 for $\varepsilon_{rad} = 1.2 \times 10^{-8}$, $a_S = 4 \times 10^5$, $a_0 = 874$, $\omega = 1$ for initial conditions: $x(0) = 0.01$, $z(0) = 0$, $p_x(0) = 0$, $p_z(0) = 0$ (red,-1); $x(0) = 0.23$, $z(0) = 0$, $p_x(0) = 0$, $p_z(0) = 0$ (blue,-2); $x(0) = 0.45$, $z(0) = 0$, $p_x(0) = 0$, $p_z(0) = 0$ (green,-3). The particle independently of the initial conditions becomes trapped by a strange attractor performing stochastic motion. Frame Fig. 24 a) shows trajectories in the (s, z) plane. As we see the electrons become trapped in the region of the ponderomotive force minimum. From Figs. 25 b) and c) with dependences of the s coordinates on time and with the trajectories in the (s, p_s, p_z) space it follows that the trapped particle motion with all the three initial conditions is irregular. As we may see in Fig. 24 d), where the Lorentz factor γ versus time for

$x(0) = 0.23$ is presented, the normalized particle energy is of the order of the dimensionless EM wave amplitude. The QED parameter χ_e , whose dependence on time for $x(0) = 0.23$ is shown in Fig. 24 e) is lower than unity, i. e. the QED effect of the recoil is weak. The Poincaré sections are shown in Fig. 24 e): the particle positions in the phase plane (p_s, p_z) at discrete times with the time step equal to the period of the driving force for $x(0) = 0.01$. As we see, the particle motion is stochastic.

Electron interaction with four colliding EM waves in the case of **the second type** particular solution corresponding to the motion along the $x = y$ direction is illustrated in Fig. 25 for $\varepsilon_{rad} = 3 \times 10^{-9}$, $a_S = 1.6 \times 10^6$, $a_0 = 3466$, $\omega = 0.25$ for initial conditions: $x(0) = 0.01$, $z(0) = 0$, $p_x(0) = 0$, $p_z(0) = 0$ (red,-1); $x(0) = 0.23$, $z(0) = 0$, $p_x(0) = 0$, $p_z(0) = 0$ (blue,-2); $x(0) = 0.45$, $z(0) = 0$, $p_x(0) = 0$, $p_z(0) = 0$ (green,-3). In this case the EM wave frequency is lower than in the above discussed case and the EM wave amplitude is higher. As a result the particle is trapped performing either regular or stochastic motion. Frame Fig. 25 a) shows trajectories in the (s, z) plane. As we see depending on the initial conditions the electron becomes trapped either in the region of the ponderomotive force maximum or in the region of its minimum. From Figs. 25 b) and c) with dependences of the s coordinates on

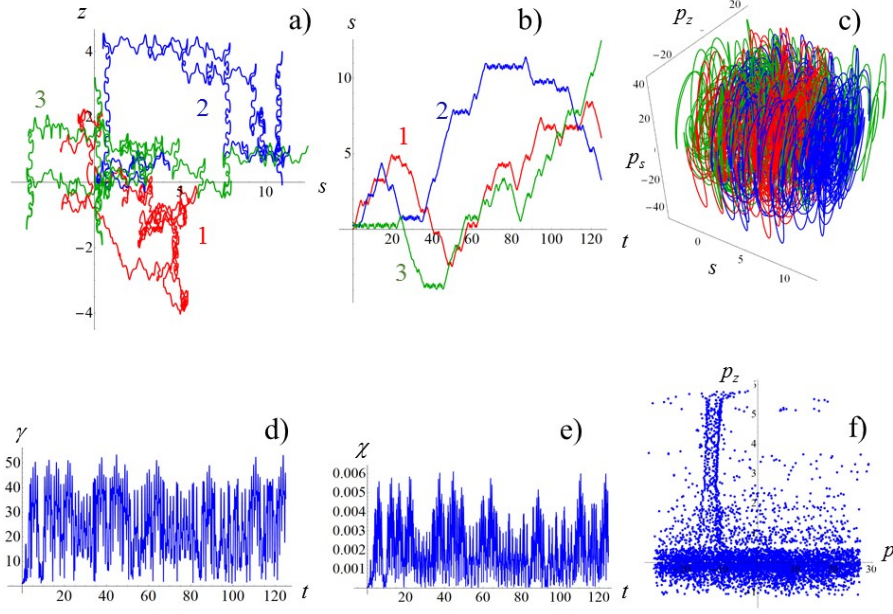


FIG. 23. Electron trajectories in the case of **the second type** particular solution corresponding to the motion along the $x = y$ direction in the field of four colliding EM waves for $\varepsilon_{rad} = 1.2 \times 10^{-8}$, $a_S = 4 \times 10^5$, $a_0 = 44$, $\omega = 1$ for initial conditions: $x(0) = 0.01$, $z(0) = 0$, $p_x(0) = 0$, $p_z(0) = 0$ (red,-1); $x(0) = 0.23$, $z(0) = 0$, $p_x(0) = 0$, $p_z(0) = 0$ (blue,-2); $x(0) = 0.45$, $z(0) = 0$, $p_x(0) = 0$, $p_z(0) = 0$ (green,-3). a) Trajectories in the (s, z) plane. b) Dependences of the s coordinates on time. c) Trajectories in the (s, p_s, p_z) space. d) The particle Lorentz factor γ versus time. e) Parameter χ versus time. f) The Poincaré sections: the particle positions in the phase plane (p_s, p_z) at discrete times with the time step equal to the period of the driving force.

time and with the trajectories in the (s, p_s, p_z) space it follows that the trapped particle motion with the initial conditions $x(0) = 0.01$ and $x(0) = 0.45$ along the limit circles is regular. As one can see in Fig. 25 d), where the Lorentz factor γ versus time for $x(0) = 0.23$ is presented, the normalized particle energy is substantially lower than the dimensionless EM wave amplitude. The QED parameter χ_e , whose dependence on time for $x(0) = 0.23$ is shown Fig. 25 e) is significantly lower than unity, i. e. the QED effect of the recoil is negligibly weak. The Poincaré sections are shown in Fig. 25 f): the particle positions in the phase plane (p_s, p_z) at discrete times with the time step equal to the period of the driving force for $x(0) = 0.23$. As we see, the particle motion along the trajectories of the attractor plotted in the inset in Fig. 25 c) with the close-up of trajectories in the (s, p_s, p_z) for $x(0) = 0.23$ is stochastic.

2. General case

The results of integration of the motion equations for the electron interacting with four s-polarized EM waves in the limit of relatively low radiation intensity are presented in Fig. 26. Fig. 26 a) shows 11 electron trajectories in the (x, y) plane for initial conditions as follows. The

initial coordinates $x(0)$ and $y(0)$ are chosen to be in the vicinity of the coordinate origin, and $z(0) = 0$, $p_x(0) = 0$, $p_y(0) = 0$, $p_z(0) = 0$. In Fig. 26 b) we show a close up of the trajectories in the vicinity of the coordinate origin superimposed with the isocontours of the electromagnetic potential averaged over a half period of the field oscillations. It is proportional to the ponderomotive potential in the high field amplitude limit, $a_0 \gg 1$. As we see, the typical trajectories are comprised of long range Lévy-flight-like excursions and of short range rambling motion, which changes the direction of the succeeding flight. Corresponding particle trajectory in the (p_x, p_y, p_z) momentum space for $x(0) = -0.125$ and $y(0) = 0.125$ is presented Fig. 26 c). According to the dependence of the parameter χ_e on time plotted in Fig. 26 d) the QED recoil effects are weak under the conditions of consideration. The Poincaré sections, the particle positions in the phase plane (p_x, p_y) at discrete times with the time step equal to the period of the driving force, in Fig. 26 e), show that the particle motion is stochastic.

Fig. 27 illustrates the particle dynamics in the EM field formed by four s-polarized EM waves for the radiation intensity higher than that intensity which corresponds to the interaction regime shown in Fig. 26. Here the electromagnetic field amplitude is $a_0 = 2823$, the dissipation parameter is $\varepsilon_{rad} = 1.2 \times 10^{-9}$, the normalized critical

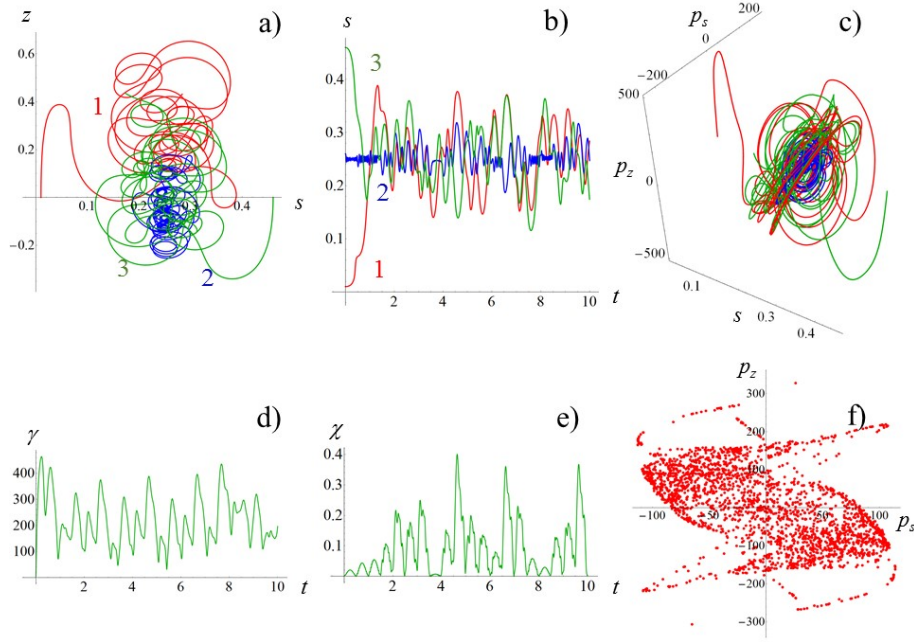


FIG. 24. Electron trajectories in the case of **the second type** particular solution corresponding to the motion along the $x = y$ direction in the field of four colliding EM waves for $\varepsilon_{rad} = 1.2 \times 10^{-8}$, $a_S = 4 \times 10^5$, $a_0 = 874$, $\omega = 1$ for initial conditions: $x(0) = 0.01$, $z(0) = 0$, $p_x(0) = 0$, $p_z(0) = 0$ (red,-1); $x(0) = 0.23$, $z(0) = 0$, $p_x(0) = 0$, $p_z(0) = 0$ (blue,-2); $x(0) = 0.45$, $z(0) = 0$, $p_x(0) = 0$, $p_z(0) = 0$ (green,-3). a) Trajectories in the (s, z) plane. b) Dependences of the s coordinates on time. c) Trajectories in the (s, p_s, p_z) space. d) Lorentz factor γ versus time for $x(0) = 0.45$. e) Parameter χ_e versus time for $x(0) = 0.45$. f) The Poincaré sections: the particle positions in the phase plane (p_s, p_z) at discrete times with the time step equal to the period of the driving force for $x(0) = 0.01$.

QED field is $a_S = 4 \times 10^6$, and the EM field frequency equals $\omega_0 = 0.1$. From Fig. 27 a) and b) it follows that the typical trajectories form a pretty regular pattern in the (x, y) plane. They are comprised of long range Lévy-flight-like excursions and of short range rambling motion, which changes the direction of the succeeding flight. The combination of the long range excursions and short range rambling is also seen in the behavior of the electron trajectory in the (x, y, z) space presented in Fig. 27 d). The corresponding particle trajectory in the (p_x, p_y, p_z) momentum space for $x(0) = -0.125$ and $y(0) = 0.125$ is presented in Fig. 27 c). What is remarkable is that during the Lévy like flights the electron moves almost along the electric node region, i.e. performing the motion described by the second type particular solution discussed above (see Figs. 24). The particle normalized energy changes from 200 to approximately 1200. The value of the QED dimensionless parameter χ_e (not shown here) is less than unity. The Poincaré sections (also not shown here) are similar to those sections which are presented in Fig. 26 e) indicating stochasticity in the electron dynamics.

Further increasing the EM field intensity and/or decreasing the field frequency lead to an intriguing change in the trajectory pattern (see Fig. 28, where an ensemble of the electron trajectories in the (x, y) plane is presented). The results presented in Figs. 28 and 29

have been obtained for the electromagnetic field amplitude of $a_0 = 11856$, for the dissipation parameter of $\varepsilon_{rad} = 6 \times 10^{-10}$, for the normalized critical QED field of $a_S = 8 \times 10^6$, and for the EM field frequency equal to $\omega_0 = 0.05$. The trajectory topology can be subdivided into two classes depending on the particle initial conditions. If the particle is initially close to the bottom of the ponderomotive potential, i.e. close to the lines $x = \pm y = \pi n$, $n = \dots, -2, -1, 0, 1, 2, \dots$ in the (x, y) plane, it remains there. The particle trajectory, in this case, is similar to those shown in Figs. 27 a) and b). The second class trajectories are realized for the initial particle positions in the vicinity of the ponderomotive potential maximum, where the magnetic field of the colliding EM waves vanishes. The second class trajectories are trapped within one of the sectors, $0 < \theta < \pi/4$, $\pi/4 < \theta < \pi/2$, etc. Oscillating along the radial direction they drift relatively slowly towards the lines either $x = 0$ or $y = 0$. In both the cases of the first and second topology classes the particles move also along the z axis as seen from the results presented in Fig. 29. The first class particle dynamics is stochastic: the trajectory in the (p_x, p_y, p_z) space plotted in Fig. 29 d) corresponds to a strange attractor while Fig. 29 b) shows that the second class dynamics is regular.

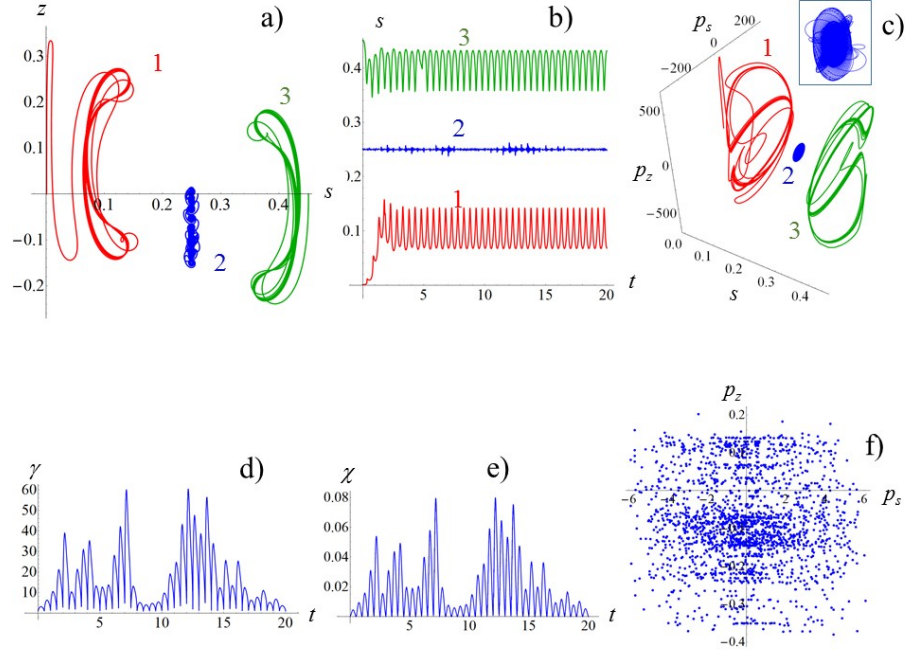


FIG. 25. Electron trajectories in the case of **the second type** particular solution corresponding to the motion along the $x = y$ direction in the field of four colliding EM waves for $\varepsilon_{rad} = 3 \times 10^{-9}$, $a_S = 1.6 \times 10^6$, $a_0 = 3466$, $\omega = 0.25$ for initial conditions: $x(0) = 0.01$, $z(0) = 0$, $p_x(0) = 0$, $p_z(0) = 0$ (red,-1); $x(0) = 0.23$, $z(0) = 0$, $p_x(0) = 0$, $p_z(0) = 0$ (blue,-2); $x(0) = 0.45$, $z(0) = 0$, $p_x(0) = 0$, $p_z(0) = 0$ (green,-3). a) Trajectories in the (s, z) plane. b) Dependences of the s coordinates on time. c) Trajectories in the (s, p_s, p_z) space. The inset shows a close-up of trajectories in the (s, p_s, p_z) for $x(0) = 0.23$. d) Lorentz factor γ versus time for $x(0) = 0.23$. e) Parameter χ_e versus time for $x(0) = 0.23$. f) The Poincaré sections: the particle positions in the phase plane (p_s, p_z) at discrete times with the time step equal to the period of the driving force for $x(0) = 0.23$.

C. Electron interaction with four p-polarized EM waves

In the case of four p-polarized colliding laser pulses the EM configuration is described by Eqs. (57), (58), (59). As in the s-polarization case, in the limit of relatively low EM wave intensity the electron performs the random walk motion comprised of short scale-length oscillations interleaved by long scale excursions. An example of such trajectories is shown in Fig. 30 a) for the EM field amplitude $a_0 = 1.6 \times 10^3$, the dissipation parameter equal to $\varepsilon_{rad} = 1.2 \times 10^{-8}$, and the normalized critical QED field of $a_S = 4.12 \times 10^5$. The curve marked by red color and the number “1” corresponds to the initial coordinates $x(0) = 0.001$ and $y(0) = 0.01$. Fig. 30 b) presents a close-up of trajectory (1) the (x, y) plane overlaid with the isocontours of the EM ponderomotive potential. Electron oscillations in the (p_x, p_y) plane (Fig. 30 c)) and dependence of the y coordinate on time plotted in Fig. 30 d) demonstrate that the particle motion is irregular. The stochastic character of the particle dynamics is also distinctly seen in the Poincaré sections in the plane (p_x, p_y) , which is presented in Fig. 30 d).

For ten times higher EM field amplitude, when $a_0 = 1.6 \times 10^4$, the particle motion becomes regular as seen

in Fig. 31. In the (x, y) plane the electron performs long range Lévy-like-flights along the lines $x = \pm y + \pm \pi n$, which end up in the localized attractors, where the particle oscillates pretty regularly (see Figs. 31 a) and b)). This electron behavior is well seen in Figs. 31 c) – e) presenting the electron trajectory in the (p_x, p_y) plane, the time dependence of the y coordinate and the Poincaré mapping in the momentum plane (p_x, p_y) , respectively. Broadening of the trajectories in the Poincaré mapping Figs. 31 e) also indicates stochastic properties present in the particle motion.

Further ten times increase of the EM field amplitude, $a_0 = 1.6 \times 10^5$, results in the particle trapping within narrow stripes localized at the bottoms of the ponderomotive potential (Figs. 32 a) and b)). A combination of regular and stochastic aspects of the particle dynamics in this case too is seen from the behavior of the electron trajectory in the (p_x, p_y) plane (Figs. 32 c)), from the time dependence of the y coordinate (Figs. 32 d)), and from the broadening of the trajectories in the Poincaré mapping (Figs. 32 d)).

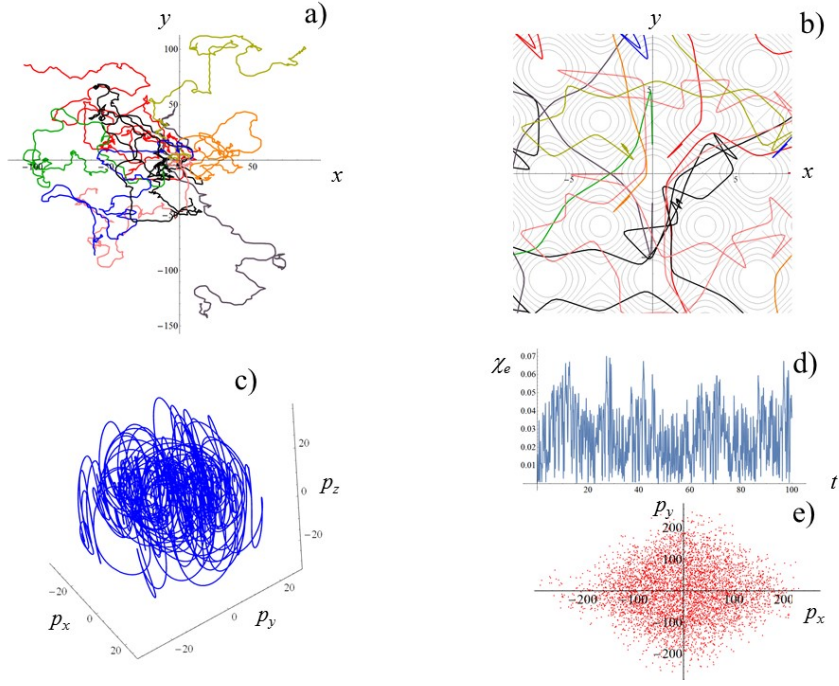


FIG. 26. a) 11 electron trajectories in the (x, y) plane for initial conditions: $x(0)$ and $y(0)$ are in the vicinity of the coordinate origin, and $z(0) = 0$, $p_x(0) = 0$, $p_y(0) = 0$, $p_z(0) = 0$. b) Close up of the trajectories in the region $(-7.5 < x < 7.5; -7.5 < y < 7.5)$. c) Trajectory in the (p_x, p_y, p_z) space. d) Parameter χ_e versus time. e) The Poincaré sections: the particle positions in the phase plane (p_x, p_y) at discrete times with the time step equal to the period of the driving force. The electromagnetic field amplitude is $a_0 = 218$, the dissipation parameter is $\varepsilon_{rad} = 1.2 \times 10^{-8}$, the normalized critical QED field is $a_S = 4 \times 10^5$, and the EM field frequency equals $\omega_0 = 1$.

VII. CONCLUSIONS

As is well known, the multiple colliding laser pulse concept [1] is beneficial for achieving extremely high amplitude of coherent electromagnetic field (see also Refs. [14–17]). The complexity of the topology of the time-dependent EM field of colliding laser pulses results in the high complexity of the trajectories of charged particles interacting with these fields. In the high field limit, when the radiation friction effects become significant, the charged particle behavior demonstrates remarkable features corresponding to random walk trajectories, Lévy flights, limit circles, attractors, and regular patterns.

In the limit of the relatively weak laser intensity, the electron motion can be described as a random walk Fig. 5 with the particle over-leaping from one field period to another. The over-leaping correspond to the Lévy flights. In contrast to the standard theory of Lévy flights, which can be found in Ref. [82–85], in the 3 and 4 colliding waves case considered in the present paper, the Lévy-like flights occur along the directions determined by the landscape of the ponderomotive potential determined in its turn by the geometry of the EM field of the colliding waves. Typically the particle performs short space scale (high frequency) oscillations intermittent with the long range leaps. This oscillation frequency appears to be significantly higher than the frequency of the driver EM

wave due to the nonlinearity of the radiation friction force (see also discussion in Refs. [27, 28]). The length of the long range flight can be found from consideration of the charged particle momentum losses due to radiation friction as in Ref. [60].

Under certain conditions (in the high intensity and/or low frequency limit) the nonlinear dissipation mechanism stabilizes the particle motion causing the particle trapping within a narrow region located near the electric field maximum. In high intensity limit the particle can be trapped in the vicinity of the EM field ponderomotive potential performing regular motion there. The particle trajectory makes regular patterns shown in Figs. 17 and 28.

We have analyzed the underlying physical mechanism of the radiating charge particle trapping in the regions of the electric field maximum. As elucidated within the framework of the simple model formulated in the present paper the particle trapping is explained by the friction drag originating from the nonlinear dependence of the radiation friction on the EM field.

The attractor trajectory patterns in Figs. 17, 19 and 27 are made by an ensemble of electrons. The single electron trajectory shown in Fig. 18 demonstrates that having been moving for a long enough time it could cover the whole attractor. In view of this, there are two questions. The first one being is there an analogy of the ergodic hy-

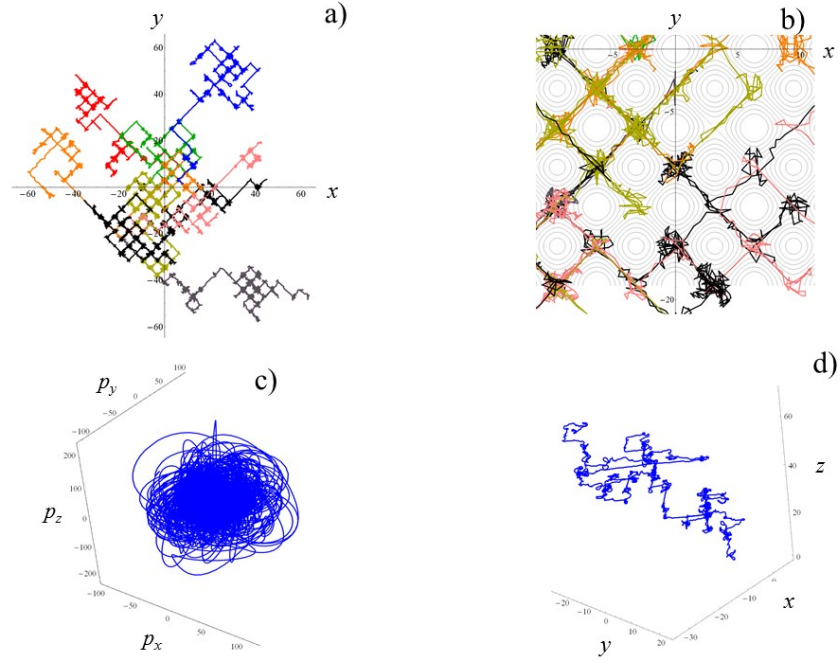


FIG. 27. a) 11 electron trajectories in the (x, y) plane for initial conditions: $x(0)$ and $y(0)$ are in the vicinity of the coordinate origin, and $z(0) = 0$, $p_x(0) = 0$, $p_y(0) = 0$, $p_z(0) = 0$. b) Close up of the trajectories in the region $(-10 < x < 10; -20 < y < 0)$ superimposed with the isocontours of the electromagnetic potential averaged over a half period of the field oscillations. c) Trajectory in the (p_x, p_y, p_z) space. d) Trajectory in the (x, y, z) space. The electromagnetic field amplitude is $a_0 = 2823$, the dissipation parameter is $\varepsilon_{rad} = 1.2 \times 10^{-9}$, the normalized critical QED field is $a_S = 4 \times 10^6$, and the EM field frequency equals $\omega_0 = 0.1$.

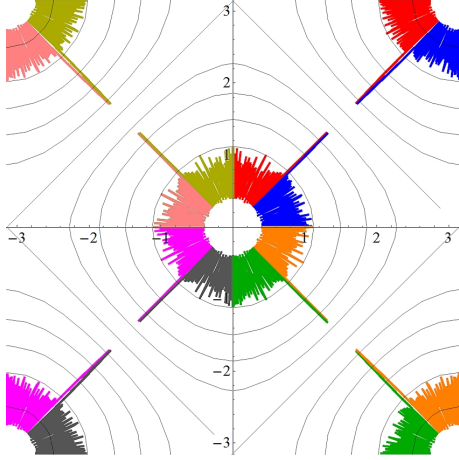


FIG. 28. Ensemble of the electron trajectories in the (x, y) plane. The particles with the initial coordinates in the region close to the $B = 0$ point are trapped inside the sectors, where their trajectories asymptotically approach the lines $x = 0$ or $y = 0$. For the initial coordinates close to the bottoms of the ponderomotive potential valleys, $x = \pm y = \pi n$, $n = \dots, -2, -1, 0, 1, 2, \dots$ the particles move along the trajectories which are similar to those shown in Figs. 27 a) and b). The EM field amplitude is $a_0 = 11856$, the dissipation parameter is $\varepsilon_{rad} = 6 \times 10^{-10}$, the normalized critical QED field is $a_S = 8 \times 10^6$, and the EM field frequency equals $\omega_0 = 0.05$.

pothesis saying that over long periods of time, the time spent in some region of the attractor is proportional to the attractor measure? The second one being is there an analogy of the Poincaré recurrence theorem ([89]) saying that the particle, after a sufficiently long but finite time, returns to a point very close to the initial point? A similar question occurs in the case of the particle random walk on whether the results of the well known random walk theory (see [90]) can be used in our case. Since finding the answers to these questions requires additional thorough consideration, we leave this to the forthcoming publications.

One of the most important findings of the present work is a revealing of a new class of regular distributions made by ensembles of the particle trajectories. They are structurally determinate patterns, as if made by tiles, formed in the high field amplitude limit when the radiation friction force drastically modifies the charged particle dynamics in the electromagnetic field as can be distinctly seen in Figs. 18, 20, 27, and 28. As for the possible practical implications of these findings, these “crystal-like” patterns are expected to be seen in the spatial distribution of the gamma-rays emitted by the electrons irradiated by the multiple high power laser pulses, which has been noticed in Refs. [32] and [33].

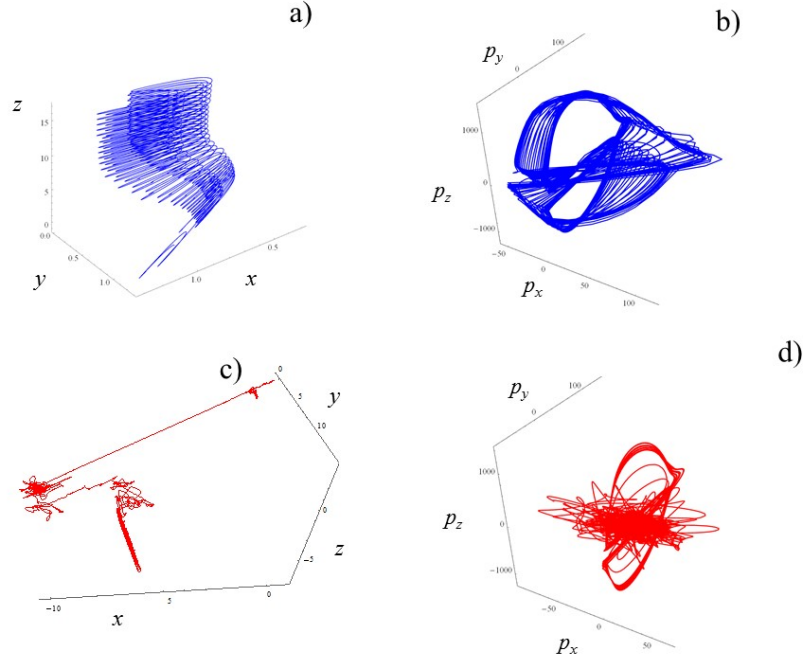


FIG. 29. a) Electron trajectory in the (x, y, z) space and b) trajectory in the (p_x, p_y, p_z) space for the **second class topology**. c) Electron trajectory in the (x, y, z) space and d) trajectory in the (p_x, p_y, p_z) space for the **first class topology**. The electromagnetic field parameters are the same as in Fig.28.

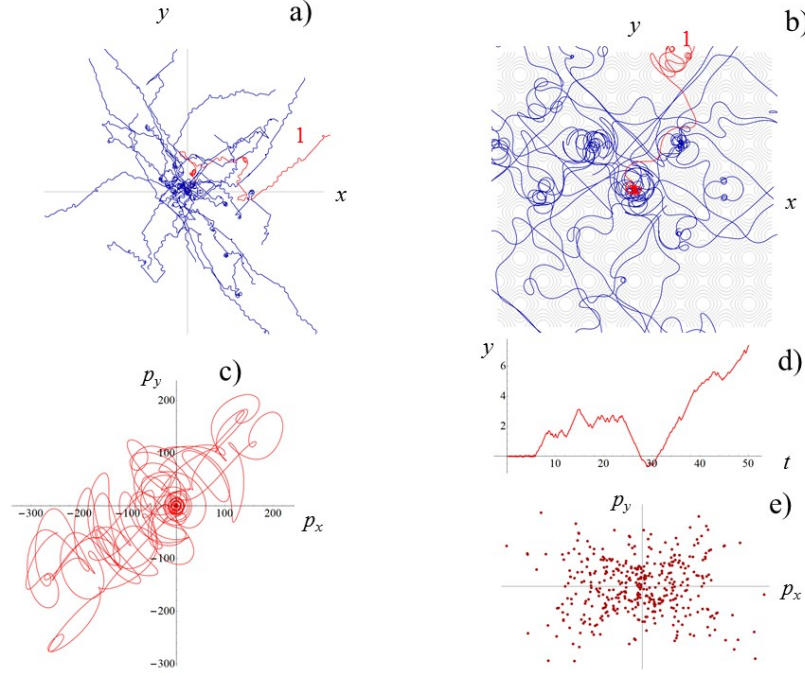


FIG. 30. Electron interaction with 4 colliding p-polarized EM waves in the low intensity limit for the electromagnetic field amplitude equal to $a_0 = 1.6 \times 10^3$, the dissipation parameter equal to $\varepsilon_{rad} = 1.2 \times 10^{-8}$, and the normalized critical QED field of $a_S = 4.12 \times 10^5$. a) Ensemble of electron trajectories in the (x, y) plane. Red color (1) curve corresponds to $x(0) = 0.001$ and $y(0) = 0.01$. b) Close-up of trajectory (1) the (x, y) plane overlaid with the isocontours of the EM field ponderomotive potential. c) Electron trajectory in the (p_x, p_y) plane. d) Coordinate y versus time t . e) The Poincaré sections: the particle positions in the phase plane (p_x, p_y) at discrete times with the time step equal to the period of the driving force.

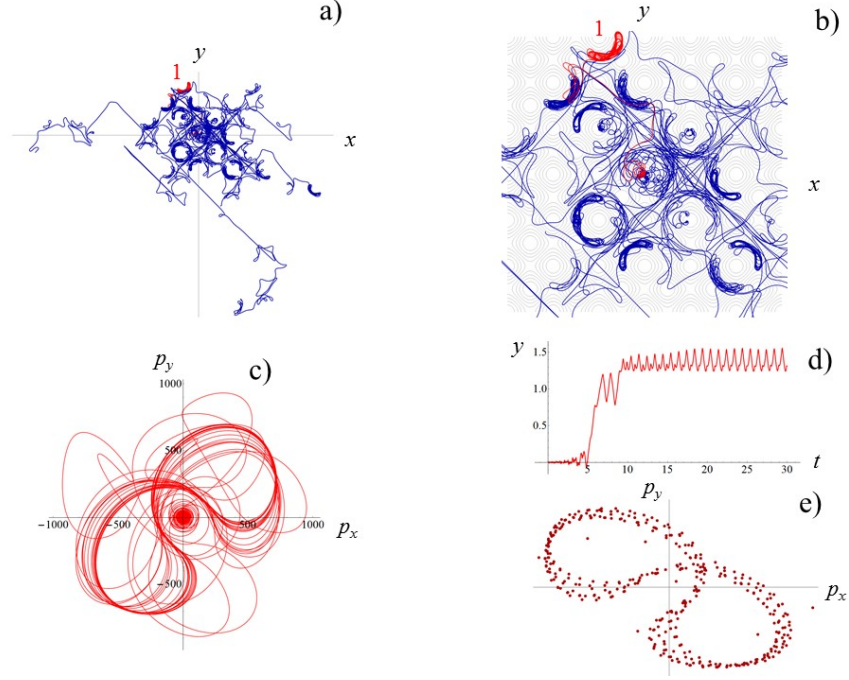


FIG. 31. The same as in Fig. 30 for $a_0 = 1.6 \times 10^4$.

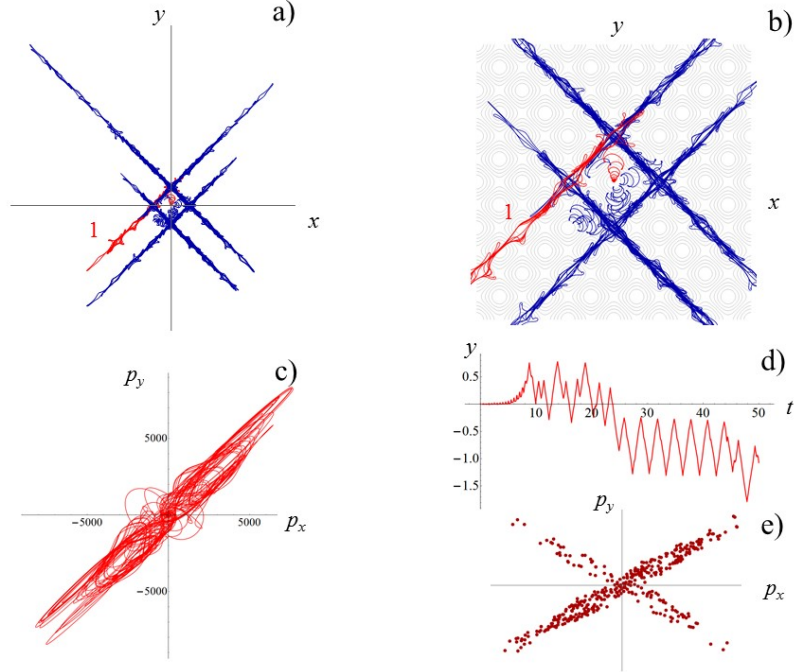


FIG. 32. The same as in Fig. 30 for $a_0 = 1.6 \times 10^5$.

ACKNOWLEDGMENTS

SSB acknowledges support from the Office of Science of the US DOE under Contract No. DE-AC02-05CH11231.

XQY and ZG acknowledge support from National Basic Research Program of China (Grant No.2013CBA01502), NSFC (Grant Nos.11535001) and National Grand Instrument Project (2012YQ030142).

-
- [1] S. S. Bulanov, V. D. Mur, N. B. Narozhny, J. Nees, and V. S. Popov, Phys. Rev. Lett. **104**, 220404 (2010).
 - [2] G. A. Mourou, G. Korn, W. Sandner, and J. L. Collier, eds., *ELI-Extreme Light Infrastructure Science and Technology with Ultra-Intense Lasers WHITEBOOK* (THOSS Media GmbH, Berlin, 2011).
 - [3] G. Mourou, T. Tajima, and S. V. Bulanov, Rev. Mod. Phys. **78**, 309 (2006).
 - [4] M. Marklund and P. Shukla, Rev. Mod. Phys. **78**, 591 (2006).
 - [5] A. Di Piazza, C. Muller, K. Z. Hatsagortsyan, and C. H. Keitel, Rev. Mod. Phys. **84**, 1177 (2012).
 - [6] Y. B. Zel'dovich, Sov. Phys. Usp. **18**, 79 (1975).
 - [7] A. G. Zhidkov, J. Koga, A. Sasaki, and M. Uesaka, Phys. Rev. Lett. **88**, 185002 (2002).
 - [8] S. V. Bulanov, T. Z. Esirkepov, J. Koga, and T. Tajima, Plasma Phys. Rep. **30**, 196 (2004).
 - [9] A. Di Piazza, Lett. Math. Phys. **83**, 305 (2008).
 - [10] C. Harvey, T. Heinzl, and M. Marklund, Phys. Rev. D **84**, 116005 (2011).
 - [11] T. Heinzl, C. Harvey, A. Ilderton, M. Marklund, S. S. Bulanov, S. Rykovanov, C. B. Schroeder, E. Esarey, and W. P. Leemans, Phys. Rev. E **91**, 023207 (2015).
 - [12] A. G. R. Thomas, C. P. Ridgers, S. S. Bulanov, B. J. Griffin, and S. P. D. Mangles, Phys. Rev. X **2**, 041004 (2012).
 - [13] A. R. Bell and J. G. Kirk, Phys. Rev. Lett. **101**, 200403 (2008).
 - [14] S. S. Bulanov, T. Esirkepov, J. Koga, A. G. R. Thomas, and S. V. Bulanov, Phys. Rev. Lett. **105**, 220407 (2010).
 - [15] I. Gonoskov, A. Aiello, S. Heugel, and G. Leuchs, Phys. Rev. A **86**, 053836 (2012).
 - [16] A. Gonoskov, I. Gonoskov, C. Harvey, A. Ilderton, A. Kim, M. Marklund, G. Mourou, and A. Sergeev, Phys. Rev. Lett. **111**, 060404 (2013).
 - [17] E. G. Gelfer, A. A. Mironov, A. M. Fedotov, V. F. Bashmakov, E. N. Nerush, I. Y. Kostyukov, and N. B. Narozhny, Phys. Rev. A **92**, 022113 (2015).
 - [18] I. M. Bassett, Optica Acta: Int. J. Optics **33**, 279 (1986).
 - [19] J. T. Mendonca, Phys. Rev. A **28**, 3592 (1983).
 - [20] D. Bauer, P. Mulser, and W. H. Steeb, Phys. Rev. Lett. **75**, 4622 (1995).
 - [21] Z.-M. Sheng, K. Mima, Y. Sentoku, M. S. Jovanovic, T. Taguchi, J. Zhang, and J. Meyer-ter Vehn, Phys. Rev. Lett. **88**, 055004 (2002).
 - [22] G. Lehmann and K. H. Spatschek, Phys. Rev. E **85**, 056412 (2012).
 - [23] G. Lehmann and K. H. Spatschek, Phys. Rev. Lett. **116**, 225002 (2016).
 - [24] A. Gonoskov, A. Bashinov, I. Gonoskov, C. Harvey, A. Ilderton, A. Kim, M. Marklund, G. Mourou, and A. Sergeev, Phys. Rev. Lett. **113**, 014801 (2014).
 - [25] A. Bashinov, A. Kim, and A. Sergeev, Phys. Rev. E **92**, 043105 (2015).
 - [26] S. V. Bulanov, T. Z. Esirkepov, M. Kando, J. Koga, K. Kondo, and G. Korn, Plasma Phys. Rep. **41**, 1 (2015).
 - [27] T. Z. Esirkepov, S. S. Bulanov, J. Koga, M. Kando, K. Kondo, N. N. Rosanov, G. Korn, and S. V. Bulanov, Phys. Lett. A **379**, 2044 (2015).
 - [28] M. Jirka, O. Klimo, S. V. Bulanov, T. Z. Esirkepov, E. Gelfer, S. S. Bulanov, S. Weber, and G. Korn, Phys. Rev. E **93**, 023207 (2016).
 - [29] J. G. Kirk, Plasma Phys. Control. Fusion **58**, 085005 (2016).
 - [30] S. S. Bulanov, N. B. Narozhny, V. D. Mur, and V. S. Popov, JETP Lett. **80**, 382 (2004).
 - [31] S. S. Bulanov, N. B. Narozhny, V. D. Mur, and V. S. Popov, JETP **102**, 9 (2006).
 - [32] M. Vranic, T. Grismayer, R. A. Fonseca, and L. O. Silva, Plasma Phys. Control. Fusion **59**, 014040 (2017).
 - [33] Z. Gong, R. H. Hu, Y. R. Shou, B. Qiao, C. E. Chen, X. T. He, S. S. Bulanov, T. Z. Esirkepov, S. V. Bulanov, and X. Q. Yan, arXiv:1609.09567v2 [physics.plasm-ph] 4 Oct 2016 (2016).
 - [34] A. Gonoskov, A. Bashinov, S. Bastrakov, E. E. Efimenko, A. Ilderton, A. Kim, M. Marklund, A. Meyerov, I. Muraviev, and A. Sergeev, arXiv:1610.06404v1 [physics.plasm-ph] 20 Oct 2016 (2016).
 - [35] C. P. Ridgers, C. S. Brady, R. Duclous, J. G. Kirk, K. Bennett, T. D. Arber, A. Robinson, and A. Bell, Phys. Rev. Lett. **108**, 165006 (2012).
 - [36] T. Nakamura, J. K. Koga, T. Z. Esirkepov, M. Kando, G. Korn, and S. V. Bulanov, Phys. Rev. Lett. **108**, 195001 (2012).
 - [37] M. C. Levy, T. G. Blackburn, N. Ratan, J. Sadler, C. P. Ridgers, M. Kasim, L. Ceurvorst, J. Holloway, M. G. Baring, A. R. Bell, S. H. Glenzer, G. Gregori, A. Ilderton, M. Marklund, M. Tabak, S. C. Wilks, and P. A. Norreys, arXiv:1609.00389v1 [physics.plasm-ph] 1 Sep 2016 (2016).
 - [38] D. J. Corvan, M. Zepf, and G. Sarri, Nuclear Instr. Meth. Phys. Res. A **829**, 291 (2016).
 - [39] S. Gales, D. L. Balabanski, F. Negoita, O. Tesileanu, C. A. Ur, D. Ursescu, and N. V. Zamfir, Phys. Scr. **91**, 093004 (2016).
 - [40] M. Tamburini, F. Pegoraro, A. Di Piazza, C. H. Keitel, and A. Macchi, New. J. Phys. **12**, 123005 (2010).
 - [41] T. V. Liseykina, S. V. Popruzhenko, and A. Macchi, New. J. Phys. **18**, 072001 (2016).
 - [42] S. Tang, N. Kumar, and C. H. Keitel, arXiv:1608.02513v1 [physics.plasm-ph] 8 Aug 2016 (2016).
 - [43] L. L. Ji, A. Pukhov, I. Y. Kostyukov, B. F. Shen, and K. Akli, Phys. Rev. Lett. **112**, 145003 (2014).
 - [44] A. I. Nikishov and V. I. Ritus, Sov. Phys. JETP **19**, 529 (1964).
 - [45] A. I. Nikishov and V. I. Ritus, Sov. Phys. JETP **19**, 1191 (1964).

- [46] V. I. Ritus, *Journal of Soviet Laser Research* **6**, 497 (1985).
- [47] N. B. Narozhnyi and M. S. Fofanov, *JETP* **83**, 14 (1996).
- [48] M. Boca and V. Florescu, *Phys. Rev. A* **80**, 053403 (2009).
- [49] F. Ehlötzky, K. Krajewska, and J. Z. Kamiński, *Rep. Prog. Phys.* **72**, 046401 (2009).
- [50] T. Heinzl, A. Ilderton, and M. Marklund, *Phys. Lett. B* **692**, 250 (2010).
- [51] T. Heinzl, D. Seipt, and B. Kämpfer, *Phys. Rev. A* **81**, 022125 (2010).
- [52] F. Mackenroth and A. Di Piazza, *Phys. Rev. A* **83**, 032106 (2011).
- [53] A. I. Titov, H. Takabe, B. Kämpfer, and H. Hosaka, *Phys. Rev. Lett.* **108**, 240406 (2012).
- [54] K. Krajewska and J. Z. Kamiński, *Phys. Rev. A* **85**, 062102 (2012).
- [55] C. Harvey, T. Heinzl, and A. Ilderton, *Phys. Rev. A* **79**, 063407 (2009).
- [56] V. B. Berestetskii, E. M. Lifshitz, and L. P. Pitaevskii, eds., *Quantum Electrodynamics* (Pergamon, New York, 1982).
- [57] L. D. Landau and E. M. Lifshitz, eds., *The Classical Theory of Field* (Pergamon, New York, 1982).
- [58] A. V. Bashinov and A. V. Kim, *Phys. Plasmas* **20**, 113111 (2013).
- [59] A. Di Piazza, K. Z. Hatsagortsyan, and C. H. Keitel, *Phys. Rev. Lett.* **105**, 220403 (2010).
- [60] S. V. Bulanov, T. Z. Esirkepov, Y. Hayashi, M. Kando, H. Kiriya, J. K. Koga, K. Kondo, H. Kotaki, A. S. Pirozhkov, S. S. Bulanov, A. G. Zhidkov, P. Chen, D. Neely, Y. Kato, N. B. Narozhny, and G. Korn, *Nuclear Instr. Meth. Phys. Res. A* **660**, 31 (2011).
- [61] A. M. Fedotov, N. B. Narozhny, G. Mourou, and G. Korn, *Phys. Rev. Lett.* **105**, 080402 (2010).
- [62] N. V. Elkina, A. M. Fedotov, I. Y. Kostyukov, M. V. Legkov, N. B. Narozhny, E. N. Nerush, and H. Ruhl, *Phys. Rev. STAB* **14**, 054401 (2011).
- [63] E. N. Nerush, A. M. Kostyukov, I. Yu. Fedotov, N. B. Narozhny, N. V. Elkina, and H. Ruhl, *Phys. Rev. Lett.* **106**, 035001 (2011).
- [64] S. S. Bulanov, C. B. Schroeder, E. Esarey, and W. P. Leemans, *Phys. Rev. A* **87**, 062110 (2013).
- [65] S. V. Bulanov, *Plasma Phys. Control. Fusion* **59**, 014029 (2017).
- [66] B. M. Bolotovskii and G. V. Voskresenskii, *Sov. Phys. Usp.* **9**, 73 (1966).
- [67] A. A. Sokolov, N. P. Klepikov, and I. M. Ternov, *Zh. Eksper. Teor. Fiz.* **23**, 632 (1952).
- [68] J. Schwinger, *Proc. Natl. Acad. Sci. U.S.A.* **40**, 132 (1954).
- [69] T. Erber, *Rev. Mod. Phys.* **38**, 626 (1966).
- [70] I. V. Sokolov, J. A. Nees, V. P. Yanovsky, N. M. Naumova, and G. A. Mourou, *Phys. Rev. E* **81**, 036412 (2010).
- [71] S. V. Bulanov, T. Z. Esirkepov, M. Kando, J. K. Koga, and S. S. Bulanov, *Phys. Rev. E* **84**, 056605 (2011).
- [72] S. Zhang, *Prog. Theor. Exper. Physics* **123**, 123A01 (2013).
- [73] A. Ilderton and G. Torgrimsson, *Phys. Rev. D* **88**, 025021 (2013).
- [74] M. Abramovitz and I. A. Stegun, eds., *Handbook of Mathematical Functions with Formulas, Graphs, and Mathematical Tables* (Dover, New York, 1964).
- [75] R. Duclos, J. G. Kirk, and A. R. Bell, *Plasma Phys. Contr. Fus.* **53**, 015009 (2011).
- [76] C. S. Brady, C. P. Ridgers, T. D. Arber, A. R. Bell, and J. G. Kirk, *Phys. Rev. Lett.* **109**, 245006 (2012).
- [77] M. Lobet, C. Ruyer, A. Debayle, E. D'Humières, M. Grech, L. Lemoine, and L. Gremillet, *Phys. Rev. Lett.* **115**, 215003 (2015).
- [78] H. X. Chang, B. Qiao, Z. Xu, X. R. Xu, C. T. Zhou, X. Q. Yan, S. Z. Wu, M. Borghesi, M. Zepf, and X. T. He, *Phys. Rev. E* **92**, 053107 (2015).
- [79] A. V. Bashinov, P. Kumar, and A. V. Kim, *arXiv:1610.08847v1 [physics.plasm-ph]* 27 Oct 2016 (2016).
- [80] T. Grismayer, M. Vranic, J. L. Martins, R. A. Fonseca, and L. O. Silva, *Phys. Plasmas* **23**, 056706 (2016).
- [81] Z. Gong, R. Hu, Y. Shou, B. Qiao, C. Chen, F. Xu, X. He, and X. Yan, *Matter and Radiation at Extremes*, in press (2016).
- [82] P. P. Lévy, *Théorie de l'addition des variables aléatoires* (2nd edn, Gauthier-Villars, Paris, 1954).
- [83] R. Metzler and J. Klafter, *Phys. Reports* **339**, 1 (2000).
- [84] G. M. Zaslavsky, *Phys. Reports* **371**, 461 (2002).
- [85] R. Metzler, A. V. Chechkin, V. Y. Gonchar, and J. Klafter, *Chaos, Solitons and Fractals* **34**, 129 (2007).
- [86] R. Durrett, *Probability. Theory and examples* (Wadsworth & Brooks/Cole, Pacific Grove, CA, 1991).
- [87] A. M. Fedotov, N. V. Elkina, E. G. Gelfer, N. B. Narozhny, and H. Ruhl, *Phys. Rev. A* **90**, 053847 (2014).
- [88] L. D. Landau and E. M. Lifshitz, *Mechanics* (Pergamon, New York, 1976).
- [89] V. I. Arnol'd, *Mathematical Methods of Classical Mechanics* (Springer, New York, 1989).
- [90] M. Kac, *Kilka zagadnien stochastycznych fizyki matematyki* (Warszawa : Panstw. Wydaw. Nauk., 1961).